Atmospheric Research 273 (2022) 106166

Contents lists available at ScienceDirect

Atmospheric Research

journal homepage: www.elsevier.com/locate/atmosres

A daily drought index-based regional drought forecasting using the Global Forecast System model outputs over China

Xia Zhang [a,b,1], Yawen Duan [a,1], Jianping Duan [a,*], Liang Chen [a], Dongnan Jian [c], Meixia Lv [a], Qing Yang [a], Zhuguo Ma [a,b]

[a] Key Laboratory of Regional Climate-Environment Research for Temperate East Asia, Institute of Atmospheric Physics, Chinese Academy of Sciences, Beijing 100029, China
[b] University of Chinese Academy of Sciences, Beijing 100049, China
[c] Plateau Atmosphere and Environment Key Laboratory of Sichuan Province, School of Atmospheric Sciences, Chengdu University of Information Technology, Chengdu 610225, China

ARTICLE INFO

Keywords:
Drought forecasting
Daily drought index
Global Forecast System
Drought events
Actual evapotranspiration
Potential evapotranspiration

ABSTRACT

Drought is a complicated climatic phenomenon occurring in the phase of water scarcity and can have devastating ecological and social impacts. Reliable drought forecasting can benefit various sectors by allowing adequate lead times for drought mitigation efforts. However, drought forecasting, especially on a short-term lead timescale (within two weeks), is still challenging. In this study, we performed regional meteorological drought forecasting at short-term lead times based on a daily drought index (Daily Evapotranspiration Deficit drought Index, DEDI) using modeling outputs from Global Forecast System (GFS) of National Centers for Environmental Prediction in typical climatic regions of China. The skills of the 3-, 5-, 10-, and 14-day lead regional DEDI forecasts were systematically evaluated by comparing with the DEDI derived from the ERA5 reanalysis datasets of European Center for Medium-Range Weather Forecasts which was used as a proxy for observations. Results show that the GFS-based DEDI forecasts can realistically characterize the spatial and temporal variations of the regional drought events that occurred in North China, Southwest China, eastern Northwest China, and Northeast China, and compare favorably to the ERA5-based DEDI. The skill of the GFS-based drought forecasts varies at different lead days. The 3- and 5-day lead forecasts present the best skill in capturing spatio-temporal variability of droughts and generally show the highest correlations and the smallest deviations. For the 10- and 14-day lead regional drought forecasts, the smoothed GFS-based DEDI could bring substantial improvements with remarkably increased correlations and reduced biases, and have skills in forecasting the dryness or wetness tendency. Notably, the GFS-based DEDI has skills in forecasting the occurrence or evolution of the regional drought events, but with a limitation in the drought magnitude evaluation. Overall, these results could be conductive to achieve the reliable regional drought forecasting and effective drought mitigation over China.

1. Introduction

Drought is a high-ranked natural hazard and can induce ecosystem degradations, crop failure, and enormous socioeconomic losses (Mishra and Singh, 2011; Wang et al., 2015; Wilhite et al., 2007; Zou et al., 2005). Skillful drought forecasting, especially the short-term lead drought forecasting, plays a crucial role in mitigating the devastating impacts of droughts on ecosystems and human communities in a timely manner (Ma et al., 2021a; Mishra and Singh, 2011; Yuan et al., 2013; Zhang et al., 2017). However, it is very challenging to develop suitable techniques for forecasting and quantifying drought characteristics, due to the enhanced inherent complexity of droughts under climate change (Li et al., 2017; Manzano et al., 2019; McKee et al., 1993; Quiring, 2009; Wang et al., 2015). In particular, short-term (within two weeks) lead drought forecasts exhibit lower skills than long-term (e.g., monthly and seasonal) lead forecasts, mainly due to the complicated responses of droughts to meteo-hydrological process on a short-term timescale (e.g., the occurrence of precipitation events) (Park et al., 2018, 2020).

* Corresponding author.
E-mail address: duanjp@tea.ac.cn (J. Duan).
[1] Xia Zhang and Yawen Duan contributed equally to this work.

https://doi.org/10.1016/j.atmosres.2022.106166
Received 1 September 2021; Received in revised form 24 March 2022; Accepted 25 March 2022
Available online 30 March 2022

Many drought metrics have been utilized to develop techniques for drought forecasting, including drought indices like self-calibrated Palmer Drought Severity Index (scPDSI) and Standardized Precipitation Evapotranspiration Index (SPEI) (Ma et al., 2020; Vicente-Serrano et al., 2010; Wang et al., 2017a, 2021; Wells et al., 2004), hydrometeorological variables like precipitation and soil moisture (Li et al., 2020; Yuan et al., 2013; Liu et al., 2008), climate indices like El Niño–Southern Oscillation and Pacific Decadal Oscillation (Mo et al., 2009; Wang et al., 2017b), as well as general circulation models and neural network models (Dikshit et al., 2021; Mishra and Singh, 2009; Morid et al., 2007). However, most of those available drought metrics were established on a monthly timescale (e.g., scPDSI) and are not realizable for the implementation of the short-term lead drought forecasting. Moreover, compared to the other drought metrics, the drought indices based on the combination of actual evapotranspiration (AET) and potential evapotranspiration (PET) could be one of promising indicators in regional drought analyses and forecasts (Anderson et al., 2007; Kim and Rhee, 2016; Otkin et al., 2015; Zhang et al., 2019, 2022). This is mainly because the evapotranspiration-type indices can explicitly account for local water storage changes to highlight dry and wet conditions through combing the potential demand of atmospheric evaporation and the actual supply of water from land surface (Dai, 2011; Hobbins et al., 2016; Kim and Rhee, 2016; McEvoy et al., 2016). Previous studies (e.g., Anderson et al., 2007; Vicente-Serrano et al., 2018; Zhang et al., 2019) have also demonstrated that the evapotranspiration-type drought indices could sensitively capture the biological changes of ecosystems in response to drought dynamics and show their superiority in describing the severity of droughts and the detrimental impacts on ecological environment when compared to the commonly used drought indices like SPEI. Based on the above situations, our previous study of Zhang et al. (2022) developed a daily drought index using the difference between AET and PET (namely, Daily Evapotranspiration Deficit drought Index, DEDI) to depict the regional droughts over China. The results demonstrated that the daily DEDI index has a good performance in characterizing regional droughts over China. However, whether the daily DEDI index has the potential to be applied to forecast the short-term regional droughts using model output datasets remains unclear.

For the daily-based DEDI short-term lead drought forecasting, numerical forecast products outputted by Global Forecast System (GFS) that provided free of charge and in real time can be utilized. In recent decades, the great progress in dynamical forecasts of GFS models has been achieved by gradual improvements in observations and assimilation systems and the understandings of atmosphere-ocean-land interactions (Barnston et al., 2012; Tian, 2012), which is crucially important for drought forecasting and mitigation as well as agriculture and water resources management (Kang and Sridhar, 2018; Mishra and Singh, 2011; Trnka et al., 2020). GFS products have been widely used to forecast the upcoming weather conditions in the operational and research work, and have been verified to have a relatively reliable forecasting skill (Mo et al., 2009; Park et al., 2020; Whitaker et al., 2008). For instance, Park et al. (2020) employed GFS products and drought indices to develop a drought-forecasting model on an 8-day timescale, and they demonstrated the effective performance of the drought-forecasting model over a part of East Asia. Mo et al. (2009) adopted GFS forecasts and drought indices to skillfully illustrate the relationships between drought and sea surface temperature anomalies. In this study, we performed the short-term (within two weeks) lead drought forecasting in different time windows (i.e., 3-, 5-, 10-, and 14-day lead) based on the daily DEDI index using GFS output datasets for finer regions over China. This distinguishes from the previous studies (e.g., Park et al., 2020) that using GFS outputs and drought indices conducted an 8-day drought forecasting over East Asia. Our results are expected to improve and complement existing drought forecasts in short-term/near-real time, and to provide a better climate service for regional drought mitigation over China.

The structures of this study are to: 1) calculate the GFS-based daily drought index and conduct bias correction of the forecasts (Section 2), 2) evaluate the performance of the GFS-based drought index for the early warning of regional droughts (Section 3), and 3) discuss the potential causes of the uncertainties in the regional drought forecasts (Section 4).

2. Drought indices, data, and methods

2.1. The DEDI index

In this study, we adopted the DEDI that developed by Zhang et al. (2022) for short-term (within 14 days) lead meteorological drought forecasting. DEDI distinguishes from the standardized evapotranspiration deficit indices that developed by Kim and Rhee (2016) and Vicente-Serrano et al. (2018) which are based on Budyko theoretical approach and probability distribution algorithm, respectively. These two drought indices primarily focus on monthly-scale drought characteristics. DEDI that focuses on a daily time scale can be used for short-term (within 14 days) lead drought forecasting, and it was constructed based on a simplified standardization algorithm. The rationality for using such an algorithm has been demonstrated in our previous study (Zhang et al., 2022). Moreover, the drought indices based on the ratio of AET to PET have been mainly applied to depict drought conditions on a monthly timescale (e.g., Anderson et al., 2007; Liu et al., 2021), while the applicability to shorter timescales (e.g., daily) could be limited because the drought indices are not defined when common PET = 0 appears in many parts of the world during winter.

2.2. SPEI calculated from site observations

Station-based SPEI was chosen to verify the performance of the DEDI derived from ERA5 reanalysis in capturing dry and wet variations. SPEI incorporates precipitation and PET to represent the climatic water balance (Begueria et al., 2014; Vicente-Serrano et al., 2010). Station observations during 1979–2019 provided by surface daily meteorological dataset (v3.0) from China Meteorological Administration were adopted to calculate SPEI values. The measurements of precipitation were directly provided by observing stations. PET values were estimated using the Penman-Monteith approach that recommended by the Food and Agriculture Organization (Allen et al., 1998). The details for the specific calculation of SPEI index in this study are the same as Zhang et al. (2022). Moreover, there are two caveats. Firstly, less than 1% of the PET series were slightly negative, which is associated with condensation processes and typically occurs when the net surface radiation is negative (Singer et al., 2021). We converted the PET values on those days to zero. Secondly, daily precipitation values were observed during 20–20 h (spanning two days), which may result in slight biases in the comparisons with ERA5-based DEDI.

2.3. ERA5 reanalysis and the derived DEDI

Due to the unavailability of AET and PET observations for the study regions, we adopted high-resolution and near-real-time ERA5 datasets to verify the GFS-based DEDI forecasting skill. ERA5 products (Hersbach et al., 2020) are the state-of-the-art reanalysis produced by the European Centre for Medium-Range Weather Forecasts. Previous studies have indicated a good performance of ERA5 data in depicting energy and water variations due to a good representation of land-surface processes and the incorporation of high-quality near surface meteorological variables (Li et al., 2021; Martens et al., 2020; Sun et al., 2020). Additionally, the relatively high quality of ERA5 evapotranspiration products when applied to China has been intensively validated (e.g., Lei et al., 2021; Li and Huang, 2021; Ma et al., 2021b).

The DEDI values were calculated using daily AET and PET from ERA5 reanalysis datasets with a resolution 0.25° by 0.25 during the period of 1979–2019. The details for the calculation of DEDI index were described in Zhang et al. (2022). The DEDI-based dry and wet

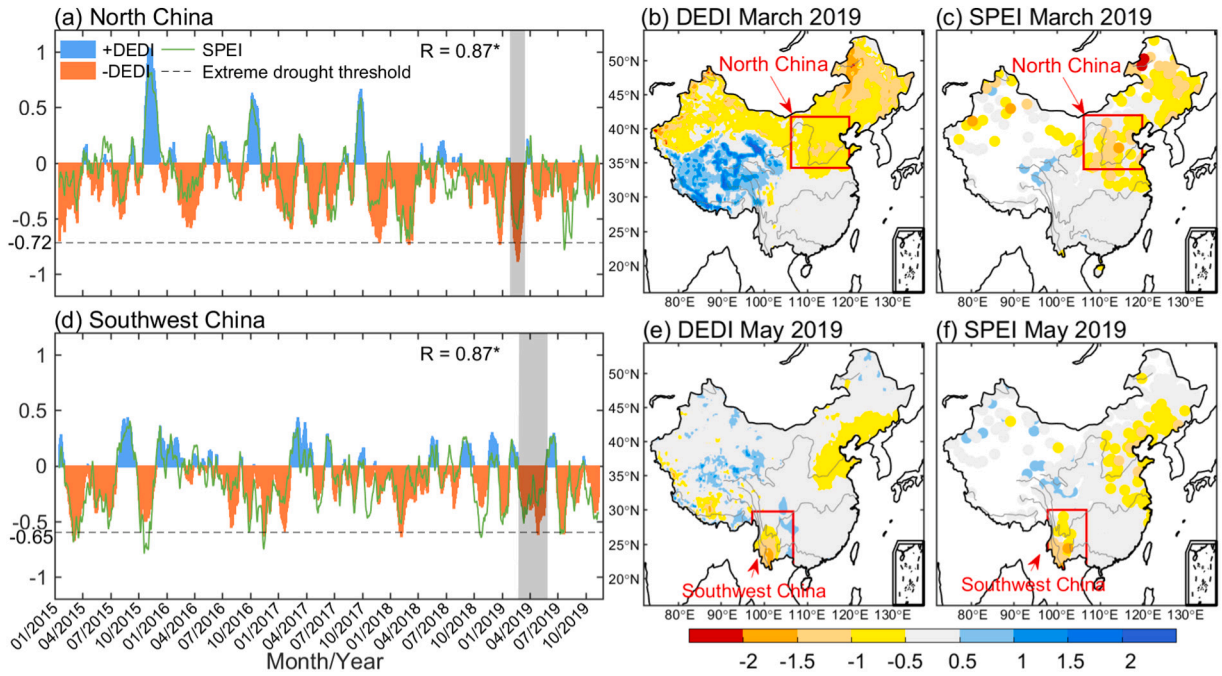

Fig. 1. Temporal evolutions in Daily Evapotranspiration Deficit drought Index (DEDI) and Standardized Precipitation Evapotranspiration Index (SPEI) during 2015–2019 in (a) North China (34–42°N, 106–120°E) and (d) Southwest China (21–30°N, 97–107°E). (b–c, e–f) Scope for the selected study area (red lines) of North China and Southwest China, respectively. The daily values of DEDI and SPEI were calculated using ERA5 reanalysis dataset and in-situ observations from China Meteorological Administration, respectively, and were smoothed on a monthly timescale in (a, d) to highlight the anomalies of the two chosen drought events. The gray shading indicates the time window of the selected drought events for the two study areas. R in (a, d) means the Pearson correlation coefficient between the DEDI and SPEI series during 2015–2019, and * denotes the correlation statistically significant at a 5% level. The colorful dots in (b, e) and (c, f) represent the spatial distribution of average daily DEDI and SPEI values, respectively, in the driest month (i.e., March 2019 for North China and May 2019 for Southwest China) of the two drought events. (For interpretation of the references to colour in this figure legend, the reader is referred to the web version of this article.)

classifications in our study regions were determined separately due to the complexity of topography and climate change across regions by referring to a percentile category approach of Svoboda et al. (2002). The detailed dry and wet classifications for the DEDI are the same as Table 2 in Zhang et al. (2022), and Tables S1–3 in this study display the smoothed DEDI classifications.

Furthermore, the quality of ERA5-based DEDI was validated via comparisons with the daily SPEI calculated using station observations (Table S4 and Fig. 1). Significantly high correlation coefficients between the observation-based SPEI and the ERA5-based DEDI both for the spatial patterns and temporal series indicate the good quality of ERA5-based DEDI. In view of the good performance of ERA5-based DEDI and near-real-time AET and PET datasets available from ERA5, the ERA5-based DEDI values were used to calibrate GFS forecasts which require to be bias-corrected using real-time data. Moreover, two points should be noted. Firstly, only the daily evolutions of droughts during the period 2015–2019 are displayed in Fig. 1a, d, because GFS products are available from 2015 and the focus of this study is verifying GFS forecasts. Secondly, DEDI detected a relatively humid condition in the Qinghai-Tibet Plateau where SPEI had lots of missing values due to the lack of observation stations, which remains unclear and requires to be verified. Considering the concerned regions of this study were not in the Qinghai-Tibet Plateau, we did not provide the additional evaluations for this area.

2.4. GFS model outputs and the DEDI forecasts

GFS is a weather forecast model developed by National Centers for Environmental Prediction (NCEP). GFS products provides latent heat flux (LH) and PET forecasts on a 0.25° × 0.25° horizontal grid spacing from 08:00 Beijing standard time (BST) January 15, 2015 (https://rda.ucar.edu/datasets/ds084.1/). GFS models are initiated at 00:00, 06:00, 12:00, and 18:00 UTC (i.e., 08:00, 14:00, and 20:00 BST, and 02:00 BST in the next day), and the outputted forecasts when the model is initiated at 08:00 BST were adopted. The original GFS forecast outputs with a 3 hourly interval from 0 to 240 and with a 12 hourly interval from 240 to 384 were aggregated into the daily data used in this study. All time-related descriptions in the following refer to Beijing local time.

The DEDI forecasts were derived from daily AET and PET data using the approach of Zhang et al. (2022). PET forecasts were provided by GFS directly, and AET forecasts were estimated from the LH that provided by GFS according to AET = LH / (2.501×10^6), where the units are mm for AET and W m^{-2} for LH (Lorenz and Kunstmann, 2012). Considering that the availability of only 6-year-long GFS forecasts starting in 2015, and the large systematic error in long-term GFS forecasts resulted from recent frequent modifications of core dynamics, model physics, and data assimilation to GFS model (Harris et al., 2020; Kleist and Ide, 2015; Zhao and Carr, 1997), the climatology of GFS forecasts could not effectively act as a baseline to standardize the evapotranspiration deficit to generate DEDI forecasts. Therefore, the difference between AET and PET derived from GFS forecasts at each grid cell was standardized by the period 1979–2008 climatic evapotranspiration deficit derived from ERA5. Additionally, considering the availability of GFS forecasts up to 16 days in advance, we chose a few time intervals (i.e., at 3-, 5-, 10-, and 14-day lead times) to perform the drought forecasting.

The calculated DEDI forecasts require to be corrected due to large model systematic errors. To remove the biases from the GFS forecasts, we implemented a bias correction approach, correcting forecasts with the past k-day mean errors, defined as follows:

$$F_{cor}(n) = F_{ori}(n) - \left\{ \sum_{i=n-k}^{n-1} [F_{ori}(i) - O(i)] \right\} \Big/ k \quad (1)$$

where F_{cor} denotes the corrected forecast, F_{ori} denotes the original

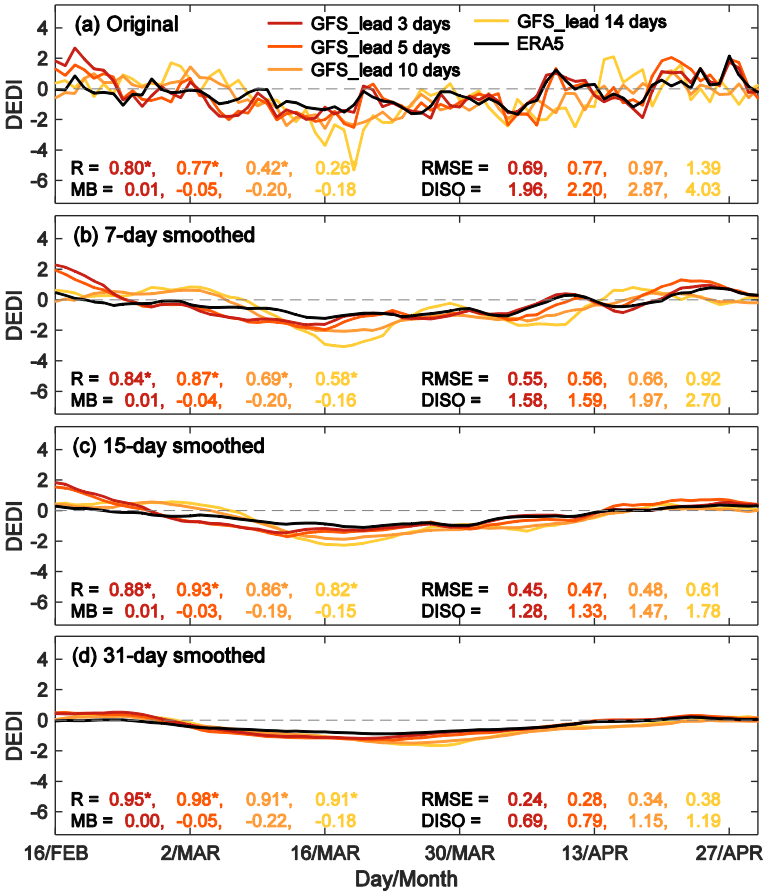

Fig. 2. Comparisons between the GFS forecasts at 3-, 5-, 10-, and 14-day lead and the ERA5-based DEDI in North China during 16 February to 30 April 2019. Comparisons in (a–d) are based on values of original, 7-day smoothed, 15-day smoothed, and 31-day smoothed, respectively. R, MB, RMSE, and DISO denote the Pearson correlation coefficient, mean bias error, root mean square error, and distance between indices of simulation and observation, respectively, between the DEDI series derived from GFS and ERA5. These values are displayed in sequence for the 3-, 5-, 10-, and 14-day lead GFS in each panel, and the * denotes the correlation statistically significant at a 5% level.

forecast, O denotes the observation, n is the day to correct the forecast, and i is the time period of mean errors. That $i > 0$ indicates the forecast or observation on the i^{th} day of current month, and that $i \leq 0$ indicates the last $|i| + 1$ day of last month, i.e., $i = 1$ denotes the first day of current month, $i = 0$ denotes the last day of last month, $i = -1$ denotes the last second days of last month, and so on. The range of k is usually 10–30 days, because the mean of the forecasting errors of larger k tends to be more robust and the values of k greater than 30 are discarded due to the interference of seasonality. Based on a series of tests, we finally adopted the mean of the past 10 days (i.e., $k = 10$) to perform forecasting bias correction (details discussed in Section 4). When k is 10, for example, the DEDI value on 30 April is corrected with the mean error from 20 April to 29 April (i.e., $n = 30$, so the range of i is 20–29). Due to the lack of observed AET and PET, we utilized the ERA5 data as a proxy for observations in this study. Further, we replaced n to n–4 in the correction of DEDI forecasts because ERA5 data are available to users within 5 days of real time. Consequently, the GFS-based DEDI forecast on 30 April was corrected with the mean error between the GFS- and ERA5-based DEDI from 16 April to 25 April.

2.5. The choice of typical drought events

Large water deficits in different regions tend to bring different agricultural and socioeconomic impacts (Ding and Gao, 2020; Funk et al., 2018; Rippey, 2015), especially in China spanning diverse topography, land cover, and climatic conditions. In this study, the drought forecasting skills at short-term lead times were evaluated through five drought events with different intensities that occurred in 2019 and 2015 in North China (34–42°N, 106–120°E), in 2019 in Southwest China (21–30°N, 97–107°E), in 2019 in eastern Northwest China (32.5–40°N, 100–107.5°E), and in 2019 in Northeast China (40–50° N, 120–130° E). The intensity of the 2015 North China drought event was weaker than the intensity of the 2019 North China drought event. The study areas of North China, eastern Northwest China, and Northeast China are located in dry and wet transition zones, and the study area of Southwest China is located in a humid zone. These areas have usually been chosen as typical regions for drought analysis (e.g., Huang et al., 2017; Li et al., 2017; Ma, 2007; Ma and Fu, 2003) due to their vulnerability to serious droughts.

In particular, North China and Southwest China experienced anomalously serious droughts in spring/summer 2019. As shown in Fig. 1, the strongest drought magnitude in recent years in North China occurred from March to April 2019. A heavy drought event occurred in Southwest China from March to July 2019 as well, and the data record (Ding and Gao, 2020) documented a record-breaking extreme drought event in Yunnan Province of Southwest China relative to the past 60 years. Moreover, the two areas are located in different parts of China (i.e., the north and south of China) and thus the two drought events are highlighted in this study.

2.6. Forecast verification measures

Pearson correlation coefficient, mean bias error, and root mean square error (RMSE) are usually applied to measure the level of agreement between two data series (Tian, 2012; Wilks, 2006; Yang et al., 2014). In addition, distance between indices of simulation and observation (DISO) (Hu et al., 2019) was adopted as a comprehensive metric that combines Pearson correlation coefficient, mean bias error, and RMSE. DISO value that approaches zero signifies a higher consistency with observation. However, DISO is invalid when observed value equals zero, due to a large difference in DISO caused by a small difference in a very close-to-zero observed value (Zhang et al., 2021). Therefore, the

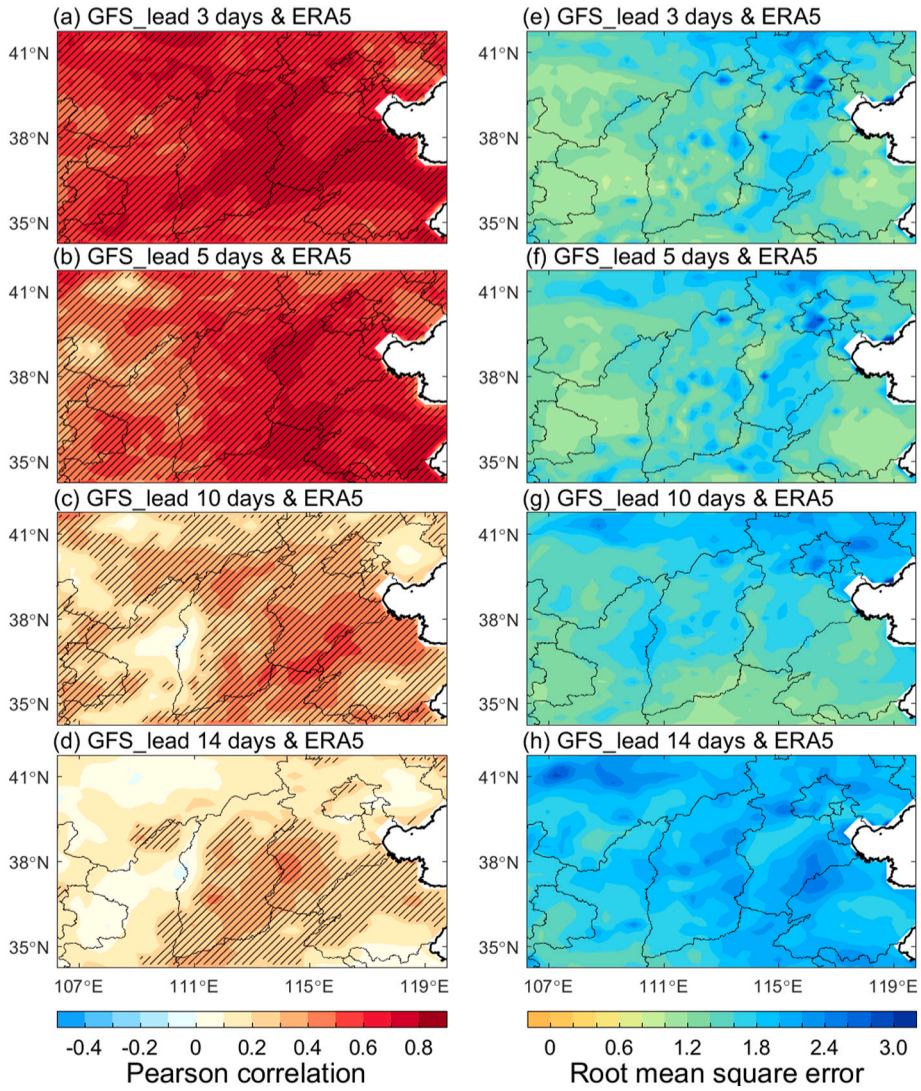

Fig. 3. Spatial patterns of (a–d) Pearson correlation coefficient, and (e–h) root mean square error between the daily DEDI series derived from GFS forecasts at 3-, 5-, 10-, and 14-day lead and ERA5 reanalysis over North China during 16 February to 30 April 2019. The hatched areas in (a–d) denote the correlation statistically significant at a 5% level.

four statistics were adopted as metrics to help objectively assess the drought forecast accuracy of GFS-based DEDI. The statistical significance of correlation was tested using a Student's *t*-test.

The reliability of categorical forecasts in terms of drought types with different intensities was evaluated using equitable threat score (ETS) (Amani et al., 2020; Tateo et al., 2019; Wilks, 2006):

$$\mathrm{ETS} = \frac{hit - a_r}{hit + miss + false\ alarm - a_r} \tag{2}$$

$$a_r = \frac{(hit + false\ alarm)(hit + miss)}{hit + miss + false\ alarm + non\_event} \tag{3}$$

where *hit* refers to that drought is forecasted and observed, *miss* denotes that observed drought is not forecasted, *false alarm* indicates that drought is forecasted but not observed, *non_event* denotes that no drought occurs in both forecast and observation, and a_r represents the proportion of correct forecasts expected by chance. The range of ETS is from −1/3 to 1.0, where 1.0 is a perfect score and below zero indicates no forecast skill.

3. Performance and skill evaluation of DEDI-based regional drought forecasting

3.1. Forecasted regional drought over North China in spring 2019

3.1.1. Forecasting skill in temporal evolutions and spatial patterns of the drought event

The temporal evolutions of daily DEDI indicate that the regional drought over North China in spring 2019 resulted from the persistent water deficits from early March to mid-April (Fig. 2). The GFS-based DEDI forecasts present a generally consistency with the DEDI derived from ERA5. All correlation coefficients between ERA5-driven DEDIs and forecasted DEDIs (including the values of original, 7-day smoothed, 15-day smoothed and 31-day smoothed) reach a 5% significance level. Drought magnitude decreases as the smoothing timescale becomes longer. The forecasted reliability varies with different lead days. The 3-day lead forecasts show the best agreement with the ERA5, while the 14-day lead forecasts present a limited skill as expressed by the lowest correlation coefficient and the largest RMSE and DISO values. This arises from the low correlation relationship between the 14-day lead forecasts and the ERA5 in most parts of the region, except for the southeastern part (Fig. 3). Correspondingly, the 14-day lead forecasts present the

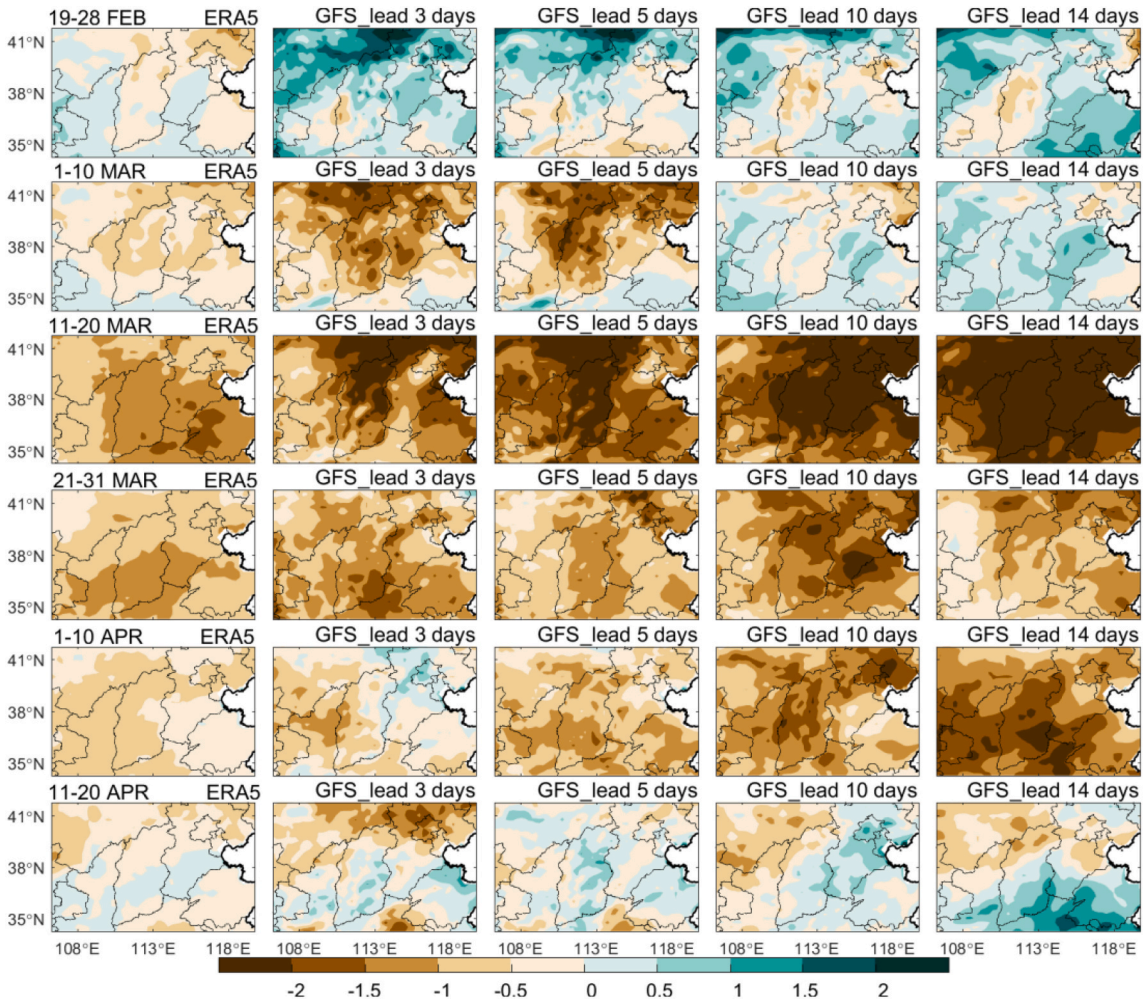

Fig. 4. Spatial comparisons of the 10-day averaged DEDI derived from ERA5 reanalysis and GFS forecasts at 3-, 5-, 10-, and 14-day lead over North China during 19 February to 20 April 2019.

largest RMSE values over the entire North China compared to the 3-, 5-, and 10-day lead forecasts. Additionally, using the smoothing technique brings substantial improvements in the 10- and 14-day lead forecasts which are originally less desirable. Particularly, the 31-day smoothed DEDIs show the same level of correlation between the GFS forecasts at different lead times and the ERA5, and they have correlation coefficients over 0.91 as well as RMSE values less than 0.38. These results suggest that the 3- and 5-day lead forecasts provide useful skills in capturing spatio-temporal variability of droughts, and the 10- and 14-day lead forecasts are appropriate for forecasting dryness or wetness tendency.

Considering that this drought event lasted about 60 days, the spatial evolutions of the 10-day averaged DEDI based on GFS forecasts and ERA5 over North China are further compared (Fig. 4). The 10-day averaged spatial pattern in the GFS forecasts, especially in lead 3 or 5 days, generally agrees with that in the ERA5. Both forecasts (in the 3- and 5-day lead) and ERA5 show an onset of the drought event over the most parts of North China in early March. The drought event intensified and reached a peak in the mid-March. Since April, the drought event began to weaken both in the intensity and the spatial scope, and most areas presented a relatively wet condition in late April. These comparisons indicate that the GFS modeling outputs, especially for the 3- and 5-day lead forecasts, have a good ability to forecast the occurrence, duration and even the intensity of drought events in North China, although a greater magnitude of drought appears in the 10- and 14-day lead forecasts. Specifically, the 3- and 5-day lead forecasts coincide with the ERA5 reanalysis (onset on 4 March), while the 10- and 14-day lead forecasts present later occurrence (outbreak on 7 March and 8 March) and overestimate intensity of the drought event. The overestimated intensity of the drought event mainly appeared in 11–20 March.

Furthermore, the series of daily correlation coefficients of the spatial patterns between the GFS forecasts and the ERA5-based DEDI (Fig. 5) quantify the forecast skills of the GFS at different lead times. The 3-day lead forecasts show the highest skill in the evolution of spatial pattern of the daily DEDI, and 89.19% daily spatial patterns of DEDI correlate significantly with the results obtained from ERA5 (Table 1). The skill of the 5-day lead forecasts for the daily evolution of DEDI also reaches at 77.03%. However, the 10- and 14-day lead forecasts show the limited skills in characterizing the evolution of drought patterns, and have lower correlations of the spatial patterns with the ERA5. After smoothing the DEDI values of the 10- and 14-day lead forecasts, the spatial correspondences between the forecasts and the ERA5 could achieve substantial improvements. The proportions of significant positive correlation ($p < 0.05$) between the forecasts in the 10- and 14-day lead and the ERA5 increase from about 57% to more than 81%.

3.1.2. Forecasting skill in intensity of the regional drought event

The area percentages of the regional daily DEDI in different intensities of moderate, severe, and extreme were used to characterize the 2019 North China spring drought event (Fig. 6). The ERA5-based regional daily DEDI shows that the drought event began to develop in late February and the drought extent expanded rapidly in early March. Large-area drought persisted from mid-March to early April and eased in

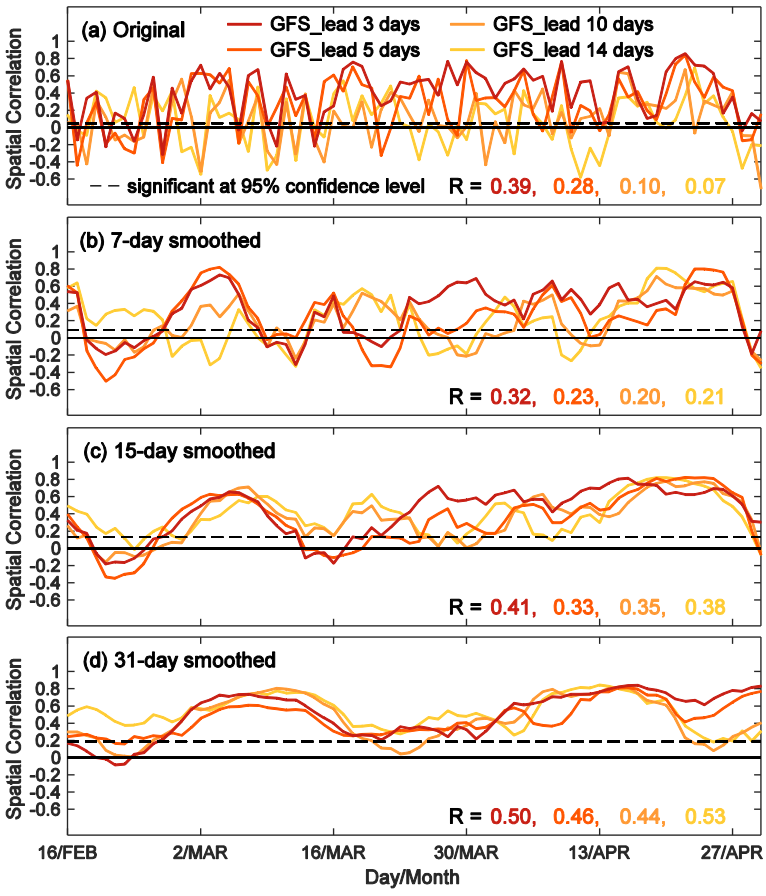

Fig. 5. Comparisons of daily correlation coefficients of the spatial patterns between the GFS forecasts at 3-, 5-, 10-, and 14-day lead and the ERA5-based DEDI in North China during 16 February to 30 April 2019. Comparisons in (a–d) are based on the DEDI values of original, 7-day smoothed, 15-day smoothed, and 31-day smoothed, respectively. R denotes the average of daily spatial correlation coefficients between the GFS- and ERA5-based DEDI, and the values are displayed in sequence for the 3-, 5-, 10-, and 14-day lead forecasts in each panel. The grey horizontal line shows denotes the threshold for correlation statistically significant at a 5% level.

Table 1
Percentage of positive correlation (R_pos) and the correlation statistically significant at a 5% level (R_sig) of the spatial patterns between the GFS-based DEDI forecasts at 3-, 5-, 10-, and 14-day lead and the ERA5 reanalysis-based DEDI in North China during 16 February to 30 April 2019.

	GFS_lead 3 days		GFS_lead 5 days		GFS_lead 10 days		GFS_lead 14 days	
	R_pos	R_sig	R_pos	R_sig	R_pos	R_sig	R_pos	R_sig
Original	89.19%	89.19%	78.38%	77.03%	64.86%	58.11%	62.16%	56.76%
7-day smoothed	79.73%	68.92%	78.38%	68.92%	75.68%	62.16%	71.62%	64.86%
15-day smoothed	85.14%	82.43%	82.43%	72.97%	89.19%	77.03%	97.30%	89.19%
31-day smoothed	95.95%	86.49%	100%	97.30%	100%	81.08%	100%	98.65%

late April. The GFS forecasts basically capture the daily variations of drought area, but overestimate the area percentage of extreme drought in North China and underestimate that of moderate and severe droughts. Compared to the 3- and 5-day lead forecasts, the 10- and 14-day lead forecasts show a later onset of the drought event and larger percentages of areas in the intensity of extreme.

To further evaluate the GFS forecasting skill in intensity of the drought event, we calculated the bias of regional average and ETS of each grid point for the regional drought event in different intensities of extreme, severe, moderate, and slight (Fig. 7). For slight, moderate, and severe droughts, the medians of the bias of regional DEDI averages between the GFS forecasts in 3-, 5-, 10-, and 14-day lead and the ERA5 approximately equal to zero (Fig. 7a). By comparison, for extreme drought, the GFS forecasts have much larger negative biases in regional DEDI averages against the ERA5, but the 3-day lead forecasts can present the smallest discrepancy from the DEDI values derived from ERA5. The biases of the regional DEDI averages for extreme drought between GFS forecasts and ERA5 exhibit more discrete distributions, as reflected by spanning a wide range of each box, implying larger tails of the DEDI values derived from GFS forecasts than those from ERA5, and thus a greater probability of forecasting extreme drought. As a result, the GFS forecasts may overestimate the area percentage of extreme drought, as shown in Fig. 6. At the same time, a greater probability of GFS forecasting extreme drought accounts for more frequent extreme drought hits, leading to the highest ETS scores for extreme drought (Fig. 7b). It is notable that the verification is rather reliable, as the ETS score integrates four possibilities including hit, false alarm, miss and correct negative, and could provide a rigorous assessment for the GFS forecasting skill (details for ETS seen in Section 2.6). Moreover, an ETS score of up to 0.33 under the threshold of slight drought (< 30% chance to occur) appears in Fig. 7b, indicating that the GFS-based DEDI could achieve a competitive skill in forecasting occurrence of regional drought.

3.2. Forecasted regional drought over Southwest China in spring and summer 2019

3.2.1. Forecasting skill in temporal evolutions and spatial patterns of the drought event

This section further evaluates the performance of the GFS-based DEDI forecasts in capturing the heavy drought event that occurred in

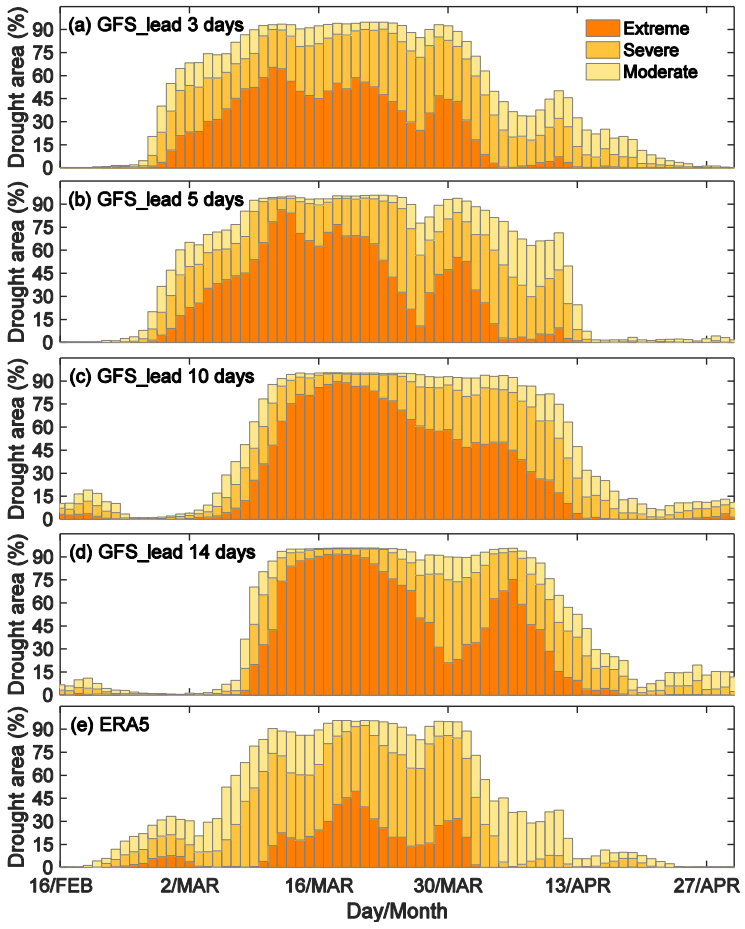

Fig. 6. Daily variations in area percentages of the regional daily DEDI in different intensities of moderate, severe, and extreme derived from the GFS forecasts at 3-, 5-, 10-, and 14-day lead and the ERA5 reanalysis in North China during 16 February to 30 April 2019. The DEDI values were smoothed on a 15-day timescale to overcome the noise from frequent dry and wet changes on a daily timescale and so to more clearly depict the drought developing from onset to demise. Light yellow, yellow, and dark yellow represent moderate, severe, and extreme drought intensities, respectively, which are stacked on top of each other. (For interpretation of the references to colour in this figure legend, the reader is referred to the web version of this article.)

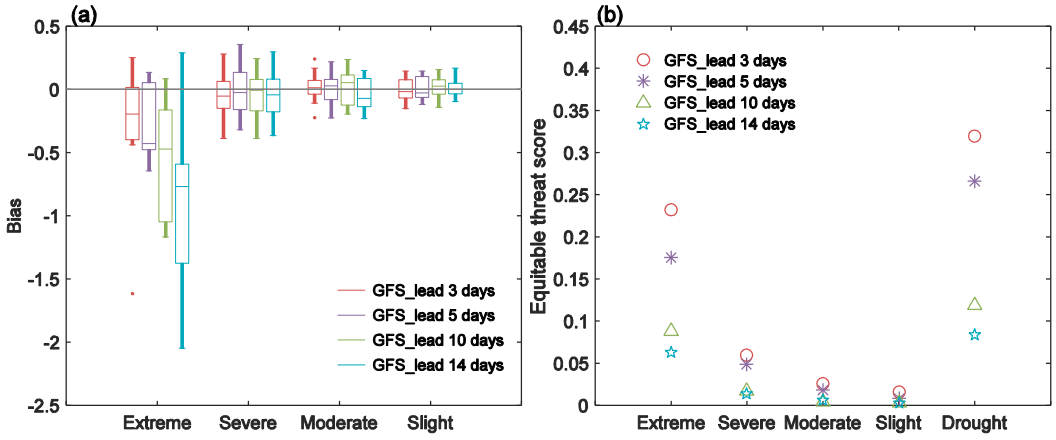

Fig. 7. (a) Bias for the regional average, and (b) equitable threat score for each grid point derived from the daily DEDI in different intensities of slight, moderate, severe, and extreme between the GFS forecasts at 3-, 5-, 10-, and 14-day lead and the ERA5 reanalysis in North China during 1 January to 30 September 2019. The box in (a) represents the interquartile range extending from the 25th quartile (bottom) to the 75th quartile (top), the central line inside the box indicates the median, the vertical lines denoting whiskers extend from the box to reach the most extreme non-outlier, and the outlying points are plotted individually. Drought in (b) denotes the situation whether a drought occurs, and the equitable threat score is obtained under the threshold of slight drought (< 30% chance to occur).

Southwest China from March to July 2019 as exhibited in Fig. 1d. The GFS forecasts present similar daily dry and wet evolutions with the ERA5 (Fig. 8), with most correlation coefficients statistically significant at a 5% level, especially for the 3- and 5-day lead forecasts. However, compared with the evaluations of drought forecasting in North China, the DEDI forecasts based on GFS are less skillful in Southwest China. Further, Fig. 9 displays the spatial distributions of the correlation between the GFS forecasts at different lead times and the ERA5. The 10- and 14-day lead forecasts have small and non-significant correlations over the most areas of Southwest China, and even negative correlation coefficients which almost do not appear in North China. In contrast, the 3- and 5-day lead forecasts achieve significant improvements in the drought forecasting skill across the whole region, but limited accuracy still appears over the western part of Southwest China as expressed by

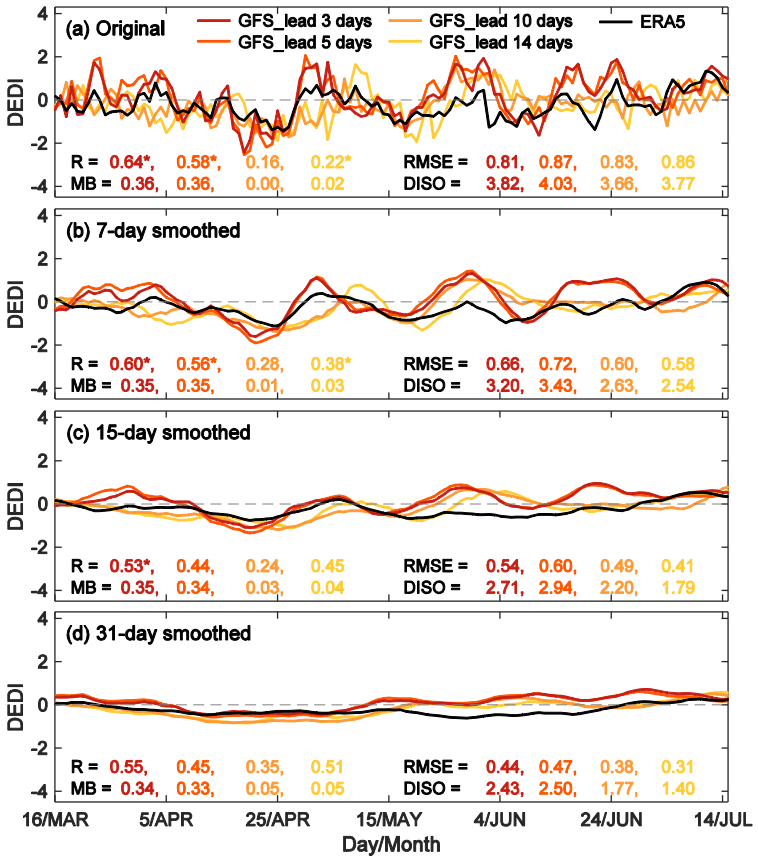

Fig. 8. Comparisons between the GFS forecasts at 3-, 5-, 10-, and 14-day lead and the ERA5-based DEDI in Southwest China during 16 March to 15 July 2019. Comparisons in (a–d) are based on values of original, 7-day smoothed, 15-day smoothed, and 31-day smoothed, respectively. R, MB, RMSE, and DISO denote the Pearson correlation coefficient, mean bias error, root mean square error, and distance between indices of simulation and observation, respectively, between the DEDI series derived from GFS and ERA5. These values are displayed in sequence for the 3-, 5-, 10-, and 14-day lead GFS in each panel, and the * denotes the correlation statistically significant at a 5% level.

most correlation coefficients of less than 0.5 as well as larger RMSE values. After smoothing the daily DEDI values on weekly, semi-monthly and monthly timescales (Fig. 8), the 10- and 14-day lead forecasts can present increased correlation coefficients and reduced RMSE and DISO values. These results verify that the potential applications of GFS-based DEDI for drought forecasting by combing the 3- and 5-day lead forecasts in capturing spatio-temporal variability of droughts and the 10- and 14-day lead forecasts in depicting dryness or wetness tendency.

Furthermore, given the around 90-day duration of the regional drought event, the spatial evolutions of the half-month averaged DEDI based on GFS forecasts and ERA5 over Southwest China are compared in Fig. 10. The spatial patterns in the GFS forecasts agree generally with those in the ERA5. Both the GFS forecasts and the ERA5 indicate that the drought occurred over central Yunnan Province from early April, and, subsequently, the intensity of drought rapidly increased in late April and the spatial extent of drought extended to almost the entire Southwest China. However, since mid-May, the ERA5-based DEDI shows that the drought sustained a relatively serious drought condition until late June, especially in Yunnan Province. By comparison, the GFS forecasts exhibit dry and wet fluctuations from mid-May. The 3- and 5-day lead forecasts indicate that the drought in Yunnan Province was significantly weakened during the second half of May, then strengthened again from early June, and, finally, eased in late June. The drought forecasted by the 10- and 14-day lead DEDI was remarkably strengthened during the second half of May, especially in the 14-day lead forecasts, and the drought began to ease in early June.

The series of correlation of the daily spatial patterns between the GFS forecasts and the ERA5-based DEDI (Fig. 11) further quantify the forecast skills of the GFS at different lead times. The 3- and 5-day lead forecasts show the highest skill in the evolution of spatial pattern of the daily DEDI, and the statistically significant correlations ($p < 0.05$) of the daily spatial patterns between the forecasts and the ERA5 account for 85.71% and 78.02% (Table 2). The smoothed 10- and 14-day lead forecasts substantially improve the skills in characterizing the evolution of drought patterns, and the proportions of significant positive correlation ($p < 0.05$) between the forecasts and the ERA5 increase from around 61% to more than 84%. Moreover, significant reductions in the spatial correlation appear in Southwest China (Fig. 11) when compared to the results in North China (Fig. 5), which is resulted from larger discrepancies of spatial pattern between the GFS forecasts at different lead times and the ERA5-based DEDI in Southwest China (Figs. 4, 10).

3.2.2. *Forecasting skill in intensity of the regional drought event*

Fig. 12 displays daily variations of the area percentage of the drought in different intensities of moderate, severe, and extreme in 2019 Southwest China spring and summer drought event. The ERA5-based regional daily DEDI shows that the drought event began to develop from mid-March, and the intensity and area of drought rapidly increased in early April. The large drought area lasted until early July, after which the magnitude and area of drought were remarkably reduced. The GFS forecasts generally capture the daily evolution of drought area. However, the GFS forecasts overestimate the area of extreme drought compared to the ERA5 and substantially underestimate the drought area in early June, which is more pronounced in the 10- and 14-day lead forecasts. Moreover, the 3- and 5-day lead forecasts show that the drought eased in late June, which is consistent with the ERA5, but at this time the 10- and 14-day lead forecasts still present relatively large areas of dry conditions.

Furthermore, the forecasting skills for the regional drought event in different intensities of extreme, severe, moderate and slight were evaluated through the bias and ETS between the GFS forecasts at different lead times and the ERA5 (Fig. 13). As the boxplots for the bias of the regional DEDI averages between the GFS forecasts and the ERA5 (Fig. 13a) exhibit, for the drought intensities in slight, moderate, and

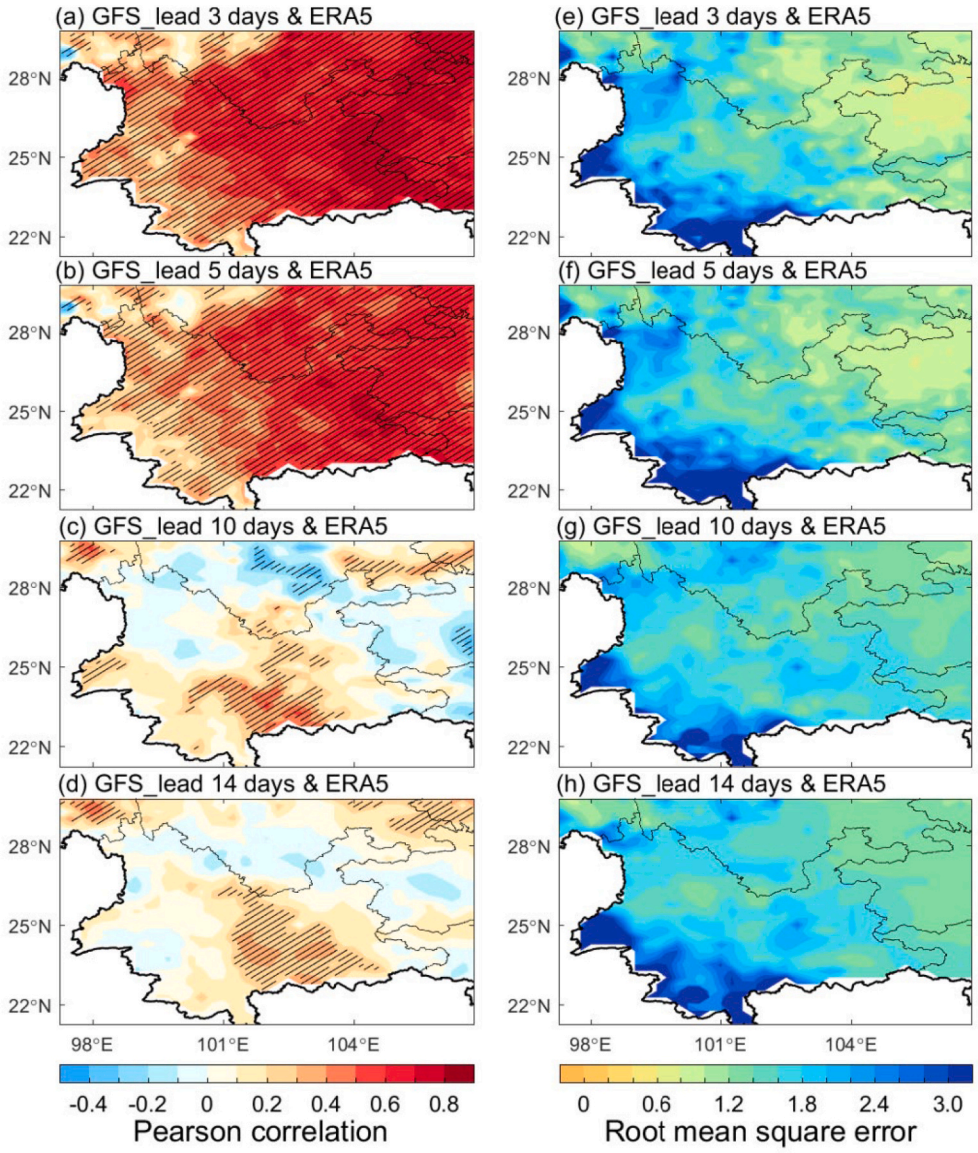

Fig. 9. Spatial patterns of (a–d) Pearson correlation coefficient, and (e–h) root mean square error between the daily DEDI series derived from GFS forecasts at 3-, 5-, 10-, and 14-day lead and ERA5 reanalysis over Southwest China during 16 March to 15 July 2019. The hatched areas in (a–d) denote the correlation statistically significant at a 5% level.

severe, the medians of the GFS forecasts and the ERA5 are approximately identical. However, for extreme drought, the GFS forecasts remarkably underestimate the regional DEDI averages compared to the ERA5, implying more occurrences of drought in the intensity of extreme in the forecasts. This corresponds to the overestimated area percentage of extreme drought as shown in Fig. 12. The 3- and 5-day lead forecasts can narrow the discrepancy of the DEDI values from the ERA5 (Fig. 13a) and obtain higher ETS scores (Fig. 13b) compared with the 10- and 14-day lead forecasts. Additionally, an ETS score of up to 0.42 under the threshold of slight drought (< 30% chance to occur) appears in Fig. 13b. These results indicate that the GFS-based DEDIs have favorable skills in forecasting whether a drought occurs, though with the limitations in distinguishing the drought magnitude in terms of extreme, severe, and moderate, which are similar to the assessments of the DEDI forecasting skills in North China.

3.3. *Forecasting skill evaluation based on three additional drought events*

To further evaluate the GFS-based DEDI drought forecasting skill, we performed further analyses based on three additional drought events that occurred in 2015 in North China, in 2019 in eastern Northwest China, and in 2019 in Northeast China.

The 2015 North China drought event (Figs. S1, S2) began to develop in early July, and then the drought intensity increased and the spatial extent rapidly expanded to most areas. The drought eased in early September, presenting wet conditions over most parts of the region. The 3- and 5-day lead GFS forecasts attain a higher consistency with the ERA5-based DEDI, presenting highly significant correlations that larger than 0.87 and smaller RMSE and DISO values. In contrast, the 10- and 14-day lead forecasts could capture the drought process, but the details of the forecasted drought do not perform well as the 3- and 5-day lead forecasts.

The 2019 eastern Northwest China drought event started from mid-March and eased in late April (Fig. S3). The 3- and 5-day lead GFS forecasts generally agree well with the ERA5-based DEDI, presenting higher correlation coefficients, reduced biases, and smaller DISO values when compared to the 10- and 14-day lead forecasts. The original and 15-day smoothed values between the ERA5- and GFS-based DEDI

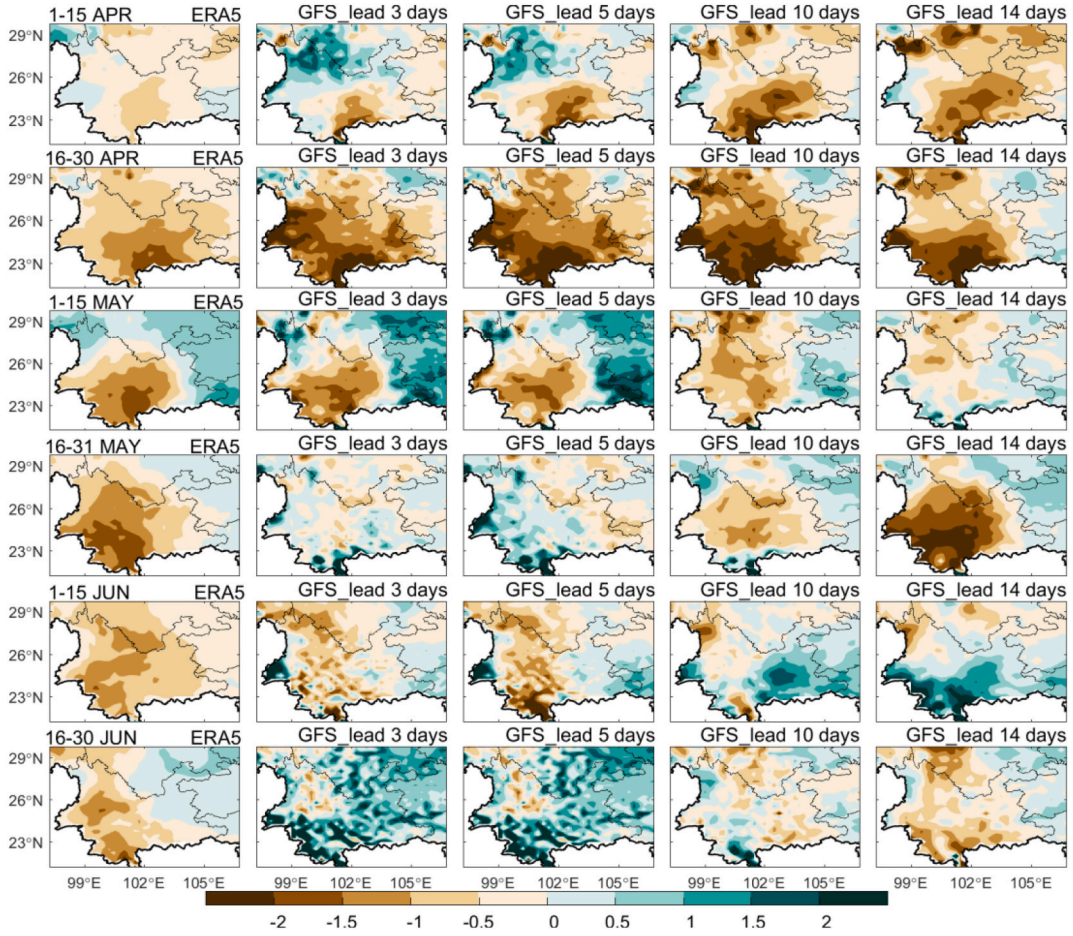

Fig. 10. Spatial comparisons of the half-month averaged DEDI derived from ERA5 reanalysis and GFS forecasts at 3-, 5-, 10-, and 14-day lead over Southwest China during 1 April to 30 June 2019.

present significant correlations ($p < 0.05$). As shown in Fig. S4, the GFS forecasts exhibit similar spatial patterns to the ERA5-based DEDI, but produce stronger intensities.

The 2019 Northeast China drought event developed from mid- to late March and eased in late May (Fig. S5). The 3- and 5-day lead GFS forecasts agree well with the ERA5-based DEDI, presenting significant correlations greater than 0.74, although the generally underestimated DEDI values appear in the GFS forecasts. Furthermore, from the forecasted spatial patterns (Fig. S6), the GFS forecasts could capture this drought process, although the forecasts at 10- and 14-day lead display a rapid jump from dry to wet at the beginning of the drought event.

In summary, the GFS-based DEDI has the capability to forecast the temporal and spatial evolutions of the 2015 North China, the 2019 eastern Northwest China, and the 2019 Northeast China drought events. The 3- and 5-day lead forecasts can realistically characterize spatio-temporal variability of droughts, and the 10- and 14-day lead forecasts have skills in depicting dryness or wetness tendency, which are similar to the evaluations in the 2019 North China and the 2019 Southwest China drought events. These results indicate the potentially effective skill of short-term lead GFS forecasts for applications in identifying droughts in various dry and wet zones.

4. Uncertainties of the DEDI based on GFS forecasts

Evaluations of Section 3 demonstrated that the GFS forecasts on a global scale produced by NCEP can provide potential benefits to short-term lead drought forecasting in China, through the comparative analyses of multiple drought events that occurred in North China, Southwest China, eastern Northwest China, and Northeast China. This section further discusses the uncertainties and deficiencies in applying the DEDI based on GFS products to drought forecasting in China.

The first is the uncertainty of the improvement in GFS forecasts by the bias correction approach adopted in this study. Despite that studies (e.g., Li et al., 2018; Linker et al., 2018; Park et al., 2020) have showed that GFS products generally have the ability to forecast the variations of atmospheric and land-surface variables such as temperature, precipitation, evapotranspiration, and soil water content, but the level of forecasting skill varies with variables, time scales, and regions. Therefore, in this study, the GFS-derived DEDI values were corrected using the bias correction approach of Eq. (1) to improve the forecast values that influenced by large model systematic errors. This method corrects the absolute values of the GFS forecasts, but retains the intrinsic nature of drought characterized by the DEDI forecasts. Take the regional droughts over North China and Southwest China in spring/summer 2019 for instance, as shown in Fig. 14. Compared to the uncorrected forecasts ($k = 0$), the corrected GFS forecasts ($k > 0$) have larger correlation coefficients and smaller RMSE values with the ERA5-based DEDI, especially in Southwest China. Additionally, Fig. 14 also shows that the length of time window to subtract forecasting errors [k in Eq. (1)] has negligible effects on the forecasting skill of the corrected GFS. The corrected GFS forecasts by subtracting forecasting errors in different time windows have approximate correlations and RMSE values with the ERA5. Therefore, we selected the first time window of 10 days to correct the bias of GFS forecasting products in Section 2.4.

The second is the uncertainty in specific drought magnitudes caused by dry and wet classification. In this study, the GFS-based DEDI shares

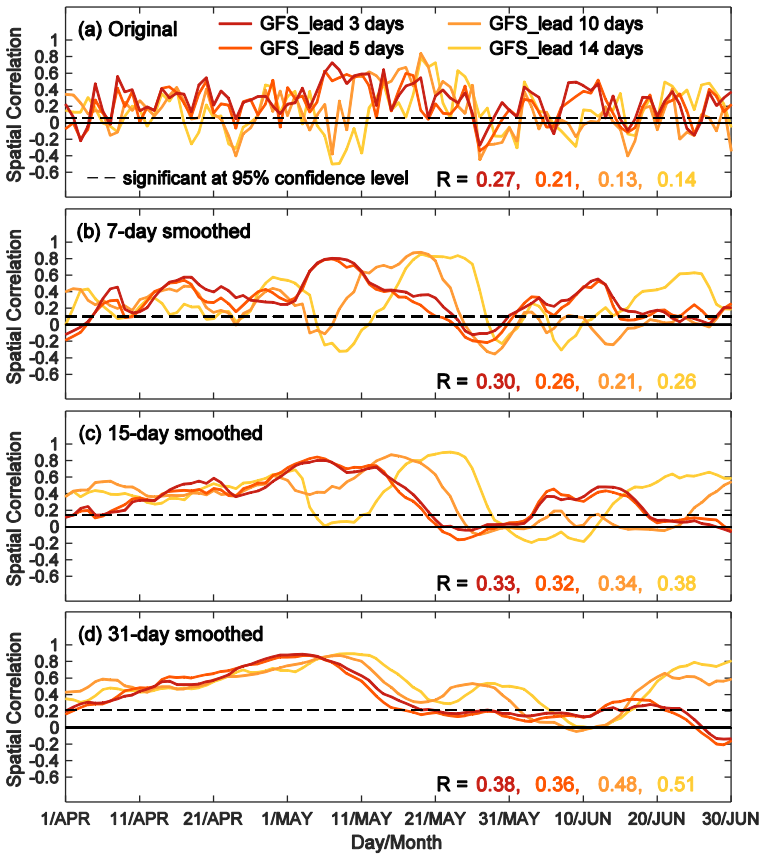

Fig. 11. Comparisons of daily correlation coefficients of the spatial patterns between the GFS forecasts at 3-, 5-, 10-, and 14-day lead and the ERA5-based DEDI in Southwest China during 1 April to 30 June 2019. Comparisons in (a–d) are based on the DEDI values of original, 7-day smoothed, 15-day smoothed, and 31-day smoothed, respectively. R denotes the average of daily spatial correlation coefficients between the GFS- and ERA5-based DEDI, and the values are displayed in sequence for the 3-, 5-, 10-, and 14-day lead forecasts in each panel. The grey horizontal line shows denotes the threshold for correlation statistically significant at a 5% level.

Table 2
Percentage of positive correlation (R_pos) and the correlation statistically significant at a 5% level (R_sig) of the spatial patterns between the GFS forecasts at 3-, 5-, 10-, and 14-day lead and the ERA5-based DEDI in Southwest China during 1 April to 30 June 2019.

	GFS_lead 3 days		GFS_lead 5 days		GFS_lead 10 days		GFS_lead 14 days	
	R_pos	R_sig	R_pos	R_sig	R_pos	R_sig	R_pos	R_sig
Original	90.11%	85.71%	84.62%	78.02%	68.13%	61.54%	69.23%	65.93%
7-day smoothed	91.21%	81.32%	89.01%	76.92%	73.63%	61.54%	83.52%	70.33%
15-day smoothed	92.31%	67.03%	90.11%	65.93%	81.32%	69.23%	86.81%	75.82%
31-day smoothed	95.60%	67.03%	94.51%	58.24%	95.60%	84.62%	98.90%	87.91%

the same magnitude threshold values of dry and wet classifications with the ERA5-based DEDI. This is resulted from the short period of freely available GFS data, and, above all, the disturbed temporal continuity of GFS model outputs due to recent modifications of model physics and data assimilation (Han and Pan, 2011; Kleist and Ide, 2015; Zhu et al., 2016). The GFS-based DEDI using the dry and wet classification can generally depict the characteristics of different drought magnitude categories. However, due to the intrinsic differences in GFS and ERA5 data which are, respectively, driven by the Finite-Volume Cubed-Sphere dynamical core (FV3) and the Integrated Forecast System (IFS) (Harris et al., 2016; Hersbach et al., 2020), the drought magnitudes identified by the GFS present deviations from those identified by the ERA5 (e.g., Fig. 6). Although the high-quality ERA5 datasets updated in nearly real time are appropriate for using in drought forecasting mentioned in this study, the high-quality evaporation products from Global Land Evaporation Amsterdam Model (GLEAM) can be used for further assessment of the uncertainty of ERA5-based DEDIs. Comparisons between DEDIs derived from ERA5 and GLEAM show a good consistence for the four typical regions selected for drought forecasting in this study (Fig. S7). Moreover, it should be noted that ERA5 products have some uncertainties in the accuracy and applicability in areas with complex terrain (Lucht et al., 2002; Martens et al., 2020) and thus may have large impacts on characterizing drought processes, which has been discussed in our previous study (Zhang et al., 2022).

The third is the uncertainty of critical variables that involved in the drought index brought by the representation of land-atmosphere interactions in numerical models. The DEDI, incorporating PET and AET, can favorably depict dry and wet conditions through taking into account atmospheric evaporative demand and actual terrestrial water storage (Hobbins et al., 2016; Kim and Rhee, 2016). Thus, the data quality for PET and AET accounts for a considerable part of the uncertainties in the DEDI forecasts. Currently, the improved performance of models in representing physical processes and incorporating assimilation techniques (Han and Pan, 2011; Kleist and Ide, 2015) can provide value-added benefits to drought forecasting. Nonetheless, in this study, compared with the evaluation of drought forecasting in North China, the DEDI forecasts are less skillful in Southwest China, which may be due to the topographic effects of Tibet Plateau and the outbreak of the summer monsoon (Song et al., 2010; Wang et al., 2014). In addition, the accuracy of drought forecasts in snow-covered areas such as Northeast China is susceptible to the model parameterization of frozen soil water that plays a vital role in evaporation during winter (Betts et al., 2001). Therefore,

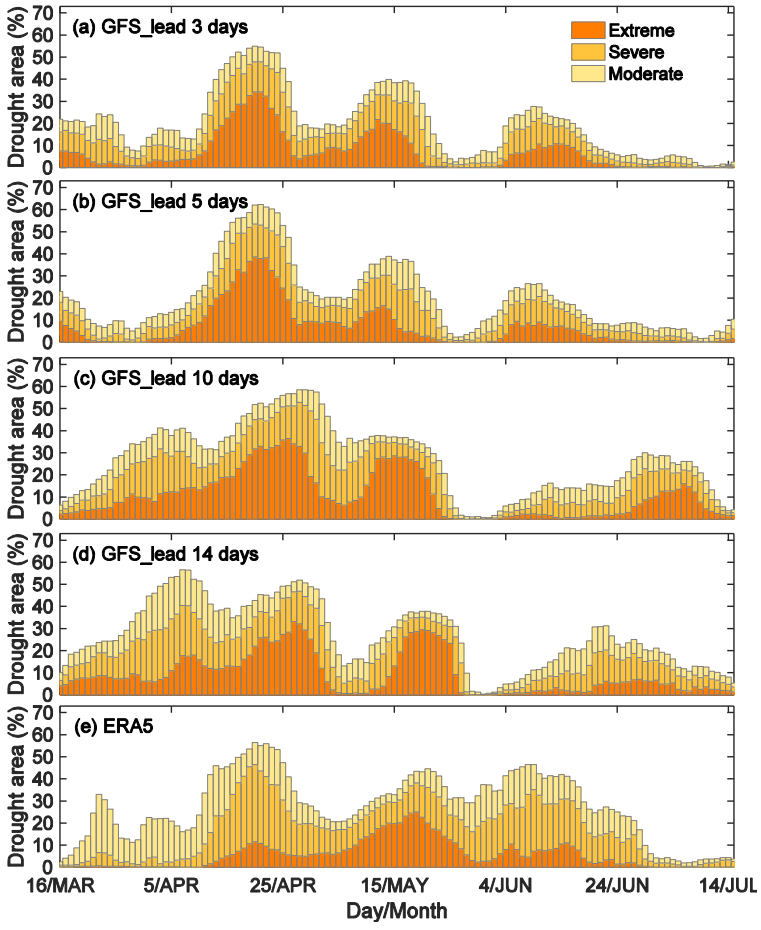

Fig. 12. Daily variations in area percentages of the regional daily DEDI in different intensities of moderate, severe, and extreme derived from the GFS forecasts at 3-, 5-, 10-, and 14-day lead and the ERA5 reanalysis in Southwest China during 16 March to 15 July 2019. The DEDI values were smoothed on a 15-day timescale to overcome the noise from frequent dry and wet changes on a daily timescale and so to more clearly depict the drought developing from onset to demise. Light yellow, yellow, and dark yellow represent moderate, severe, and extreme drought intensities, respectively, which are stacked on top of each other. (For interpretation of the references to colour in this figure legend, the reader is referred to the web version of this article.)

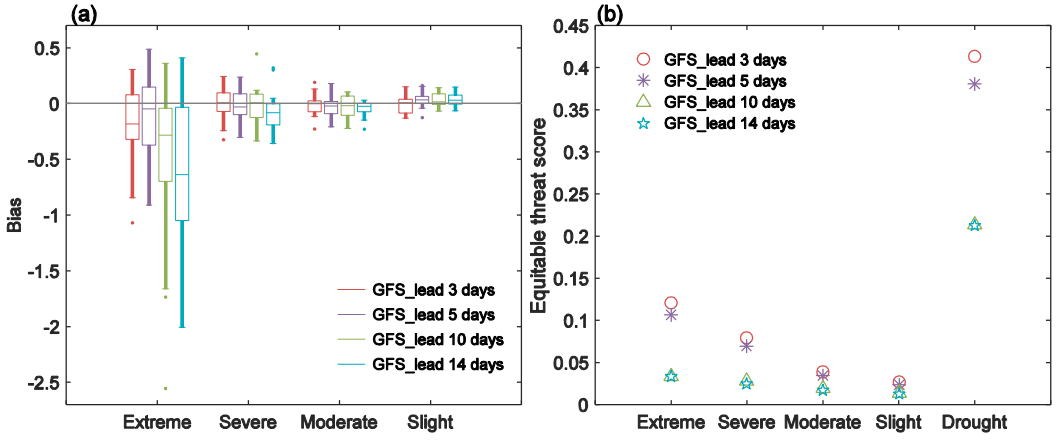

Fig. 13. (a) Bias for the regional average, and (b) equitable threat score for each grid point derived from the daily DEDI in different intensities of slight, moderate, severe, and extreme between the GFS forecasts at 3-, 5-, 10-, and 14-day lead and the ERA5 reanalysis in Southwest China during 1 January to 30 September 2019. The box in (a) represents the interquartile range extending from the 25th quartile (bottom) to the 75th quartile (top), the central line inside the box indicates the median, the vertical lines denoting whiskers extend from the box to reach the most extreme non-outlier, and the outlying points are plotted individually. Drought in (b) denotes the situation whether a drought occurs, and the equitable threat score is obtained under the threshold of slight drought (< 30% chance to occur).

more details need to be confirmed in verifying the applicability of the DEDI in practical drought forecasting.

Finally, the GFS forecasts were adopted in this study to achieve relatively reliable drought detectability. However, because all models are imperfect and no single model is expected to perform well under all circumstances, multi-model ensemble methods (Li et al., 2017; Mo and Lyon, 2015; Yuan and Wood, 2013) may be as an alternative way to achieve a better forecast skill in the future research. Furthermore, this study focuses on assessing the forecasting skill of GFS products to regional drought events, and the complicated mechanisms behind various regional drought forecasting should be explored in our future research.

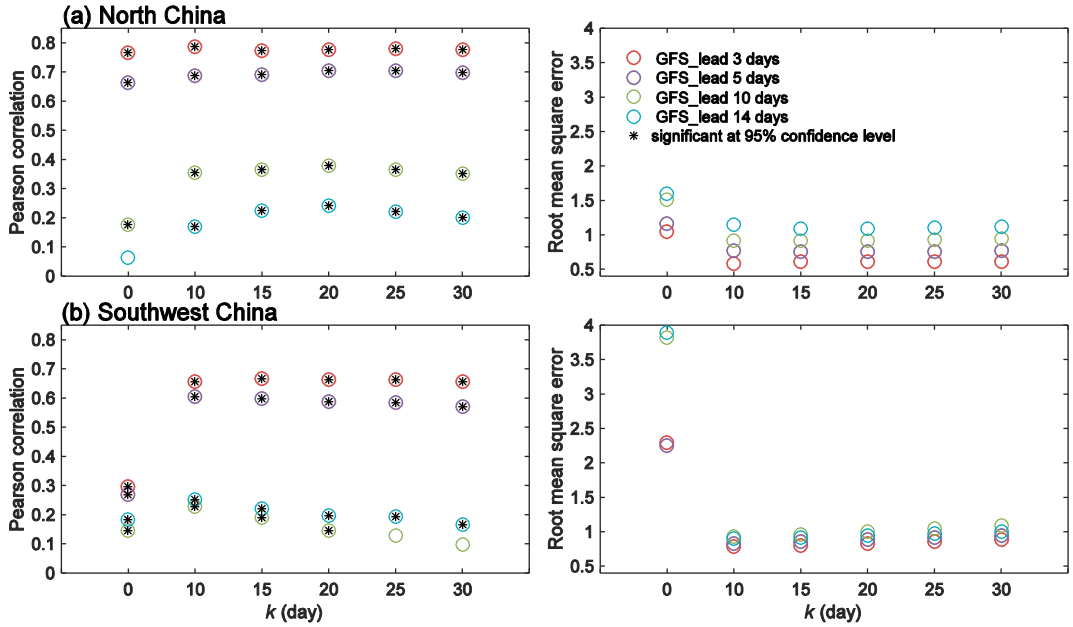

Fig. 14. Pearson correlation and root mean square error between the DEDI series derived from ERA5 reanalysis and GFS forecasts corrected by subtracting forecasting errors in different time windows [k; Eq. (1)] for (a) North China, and (b) Southwest China during 1 January to 30 September 2019. $k = 0$ indicates the original DEDI values calculated from GFS forecasts, and $k > 0$ denotes the corrected DEDI forecasts.

5. Conclusions

Based on a daily evapotranspiration deficit drought index (DEDI), we assessed the forecasting skill of regional droughts in China using Global Forecast System (GFS) outputs. The 3-, 5-, 10-, and 14-day lead DEDIs were applied to forecast multiple regional drought events that occurred in North China, Southwest China, eastern Northwest China, and Northeast China.

The GFS forecasts can reasonably depict the evolution of these regional drought events. The 3- and 5-day lead forecasts show better agreements with observations (i.e., the ERA5), while the 10- and 14-day lead forecasts have a relatively weak skill. For the 10- and 14-day lead regional drought forecasts, the smoothed GFS-based DEDI could bring substantial improvements with remarkably increased correlations and reduced RMSE values. Therefore, the 3- and 5-day lead forecasts provide useful skills in capturing spatio-temporal variability of droughts, and the 10- and 14-day lead forecasts are appropriate for forecasting dryness or wetness tendency. Notably, the GFS-based DEDI has skills in forecasting occurrence of regional drought, but with a limitation in the drought magnitude evaluation.

This study suggests that the GFS-based DEDI is helpful for reliable regional drought forecasting. To enable the universal applicability of DEDI forecasts, the assessment of multi-model ensembles across various regions should be further conducted in the future. In addition, the complicated mechanisms behind various regional drought forecasting should be further explored.

Author statement

Xia Zhang: Software, Validation, Writing - Original Draft, Writing - Review & Editing, Visualization, Methodology, Investigation.

Yawen Duan: Software, Validation, Resources, Investigation, Methodology , Visualization, Funding acquisition.

Jianping Duan: Conceptualization, Supervision, Methodology, Writing - Original Draft, Writing - Review & Editing, Funding acquisition , Project administration.

Liang Chen: Resources.

Dongnan Jian: Software, Methodology, Validation.

Meixia Lv: Funding acquisition.

Qing Yang: Resources.

Zhuguo Ma: Supervision.

Declaration of Competing Interest

The authors declare that they have no known competing financial interests or personal relationships that could have appeared to influence the work reported in this paper.

Acknowledgments

This research was funded by National Key Research and Development Program of China (2018YFC1508701). We acknowledge the Global Forecast System (GFS) products from the National Centers for Environmental Prediction (NCEP) (https://rda.ucar.edu/datasets/ds084.1/), the ERA5 reanalysis from the European Centre for Medium-Range Weather Forecasts (ECMWF) (https://www.ecmwf.int/en/forecasts/datasets/reanalysis-datasets/era5), and the surface daily meteorological station data provided by the China Meteorological Administration (http://data.cma.cn/).

Appendix A. Supplementary data

Supplementary data to this article can be found online at https://doi.org/10.1016/j.atmosres.2022.106166.

References

Allen, R.G., Pereira, L.S., Raes, D., Smith, M., 1998. Crop evapotranspiration: Guidelines for computing crop water requirements. In: FAO Irrig. Drain. Pap. No. 56. Rome 300. D05109.

Amani, M., Mahdavi, S., Bullock, T., Beale, S., 2020. Automatic nighttime sea fog detection using GOES-16 imagery. Atmos. Res. 238, 1–11. https://doi.org/10.1016/j.atmosres.2019.104712.

Anderson, M.C., Norman, J.M., Mecikalski, J.R., Otkin, J.A., Kustas, W.P., 2007. A climatological study of evapotranspiration and moisture stress across the continental United States based on thermal remote sensing: 2. Surface moisture climatology. J. Geophys. Res. Atmos. 112 https://doi.org/10.1029/2006JD007507.

Barnston, A.G., Tippett, M.K., L'Heureux, M.L., Li, S.H., DeWitt, D.G., 2012. Skill of real-time seasonal ENSO model predictions during 2002-11 is our capability increasing? Bull. Am. Meteorol. Soc. 93, 631–651. https://doi.org/10.1175/bams-d-11-00111.1.

Begueria, S., Vicente-Serrano, S.M., Reig, F., Latorre, B., 2014. Standardized precipitation evapotranspiration index (SPEI) revisited: parameter fitting, evapotranspiration models, tools, datasets and drought monitoring. Int. J. Climatol. 34, 3001–3023. https://doi.org/10.1002/joc.3887.

Betts, A.K., Viterbo, P., Beljaars, A.C.M., van den Hurk, B.J.J.M., 2001. Impact of BOREAS on the ECMWF forecast model. J. Geophys. Res. Atmos. 106, 33593–33604. https://doi.org/10.1029/2001JD900056.

Dai, A., 2011. Characteristics and trends in various forms of the Palmer Drought Severity Index during 1900–2008. J. Geophys. Res. Atmos. 116, 1–26.

Dikshit, A., Pradhan, B., Alamri, A.M., 2021. Long lead time drought forecasting using lagged climate variables and a stacked long short-term memory model. Sci. Total Environ. 755, 12. https://doi.org/10.1016/j.scitotenv.2020.142638.

Ding, T., Gao, H., 2020. The record-breaking extreme drought in yunnan province, Southwest china during spring-early summer of 2019 and possible causes. J. Meteorol. Res. 34, 997–1012. https://doi.org/10.1007/s13351-020-0032-8.

Funk, C., Harrison, L., Shukla, S., Pomposi, C., Galu, G., Korecha, D., Husak, G., Magadzire, T., Davenport, F., Hillbruner, C., Eilerts, G., Zaitchik, B., Verdin, J., 2018. Examining the role of unusually warm Indo-Pacific sea-surface temperatures in recent African droughts. Q. J. R. Meteorol. Soc. 144, 360–383. https://doi.org/10.1002/qj.3266.

Han, J., Pan, H.L., 2011. Revision of convection and vertical diffusion schemes in the NCEP Global Forecast System. Weather Forecast. 26, 520–533. https://doi.org/10.1175/waf-d-10-05038.1.

Harris, L.M., Lin, S.-J., Tu, C., 2016. High-Resolution Climate Simulations Using GFDL HiRAM with a Stretched Global Grid. J. Clim. 29, 4293–4314. https://doi.org/10.1175/JCLI-D-15-0389.1.

Harris, L., Zhou, L., Lin, S.J., Chen, J.H., Chen, X., Gao, K., Morin, M., Rees, S., Sun, Y., Tong, M., Xiang, B., Bender, M., Benson, R., Cheng, K.Y., Clark, S., Elbert, O.D., Hazelton, A., Huff, J.J., Kaltenbaugh, A., Liang, Z., Marchok, T., Shin, H.H., Stern, W., 2020. GFDL SHiELD: A unified system for weather-to-seasonal prediction. J. Adv. Model. Earth Syst. 12, 1–25. https://doi.org/10.1029/2020MS002223.

Hersbach, H., Bell, B., Berrisford, P., Hirahara, S., Horanyi, A., Munoz-Sabater, J., Nicolas, J., Peubey, C., Radu, R., Schepers, D., Simmons, A., Soci, C., Abdalla, S., Abellan, X., Balsamo, G., Bechtold, P., Biavati, G., Bidlot, J., Bonavita, M., De Chiara, G., Dahlgren, P., Dee, D., Diamantakis, M., Dragani, R., Flemming, J., Forbes, R., Fuentes, M., Geer, A., Haimberger, L., Healy, S., Hogan, R.J., Holm, E., Janiskova, M., Keeley, S., Laloyaux, P., Lopez, P., Lupu, C., Radnoti, G., de Rosnay, P., Rozum, I., Vamborg, F., Villaume, S., Thepaut, J.N., 2020. The ERA5 global reanalysis. Q. J. R. Meteorol. Soc. 146, 1999–2049. https://doi.org/10.1002/qj.3803.

Hobbins, M.T., Wood, A., McEvoy, D.J., Huntington, J.L., Morton, C., Anderson, M., Hain, C., 2016. The evaporative demand drought index. Part I: Linking drought evolution to variations in evaporative demand. J. Hydrometeorol. 17, 1745–1761. https://doi.org/10.1175/jhm-d-15-0121.1.

Hu, Z.Y., Chen, X., Zhou, Q.M., Chen, D.L., Li, J.F., 2019. DISO: A rethink of Taylor diagram. Int. J. Climatol. 39, 2825–2832. https://doi.org/10.1002/joc.5972.

Huang, J., Li, Y., Fu, C., Chen, F., Fu, Q., Dai, A., Shinoda, M., Ma, Z., Guo, W., Li, Z., Zhang, L., Liu, Y., Yu, H., He, Y., Xie, Y., Guan, X., Ji, M., Lin, L., Wang, S., Yan, H., Wang, G., 2017. Dryland climate change: Recent progress and challenges. Rev. Geophys. 55, 719–778. https://doi.org/10.1002/2016rg000550.

Kang, H., Sridhar, V., 2018. Improved drought prediction using near real-time climate forecasts and simulated hydrologic conditions. Sustainability 10, 1–29. https://doi.org/10.3390/su10061799.

Kim, D., Rhee, J., 2016. A drought index based on actual evapotranspiration from the Bouchet hypothesis. Geophys. Res. Lett. 43, 10277–10285. https://doi.org/10.1002/2016gl070302.

Kleist, D.T., Ide, K., 2015. An OSSE-based evaluation of hybrid variational-ensemble data assimilation for the NCEP GFS. Part I: System description and 3D-hybrid results. Mon. Weather Rev. 143, 433–451. https://doi.org/10.1175/mwr-d-13-00351.1.

Lei, Y.H., Shi, J.C., Xiong, C.A., Ji, D., 2021. Tracking the Atmospheric-Terrestrial Water Cycle over the Tibetan Plateau Based on ERA5 and GRACE. J. Clim. 34, 6459–6471. https://doi.org/10.1175/JCLI-D-20-0692.1. WE - Science Citation Index Expanded (SCI-EXPANDED).

Li, X.Z., Huang, W.R., 2021. How long should the pre-existing climatic water balance be considered when capturing short-term wetness and dryness over China by using SPEI? Sci. Total Environ. 786 https://doi.org/10.1016/j.scitotenv.2021.147575. WE - Science Citation Index Expanded (SCI-EXPANDED).

Li, W.T., Duan, Q.Y., Miao, C.Y., Ye, A.Z., Gong, W., Di, Z.H., 2017. A review on statistical postprocessing methods for hydrometeorological ensemble forecasting. Wiley Interdiscip. Rev. 4, 1–24. https://doi.org/10.1002/wat2.1246.

Li, D.Z., Franssen, H.J.H., Han, X.J., Jimenez-Bello, M.A., Alzamora, F.M., Vereecken, H., 2018. Evaluation of an operational real-time irrigation scheduling scheme for drip irrigated citrus fields in Picassent. Spain. Agric. Water Manag. 208, 465–477. https://doi.org/10.1016/j.agwat.2018.06.022.

Li, M.X., Wu, P.L., Ma, Z.G., Lv, M.X., Yang, Q., 2020. Changes in soil moisture persistence in China over the past 40 years under a warming climate. J. Clim. 33, 9531–9550. https://doi.org/10.1175/jcli-d-19-0900.1.

Li, M., Wu, P., Sexton, D.M.H., Ma, Z., 2021. Potential shifts in climate zones under a future global warming scenario using soil moisture classification. Clim. Dyn. 56, 2071–2092. https://doi.org/10.1007/s00382-020-05576-w.

Linker, R., Sylaios, G., Tsakmakis, I., Ramos, T., Simionesei, L., Plauborg, F., Battilani, A., 2018. Sub-optimal model-based deficit irrigation scheduling with realistic weather forecasts. Irrig. Sci. 36, 349–362. https://doi.org/10.1007/s00271-018-0592-x.

Liu, L., Sun, L., Liao, Y., Zhu, Y., Zou, X., Wang, Y., Yan, J., 2008. Development and application of national prediction system for extreme high temperature. Meteorol. Monogr. 34, 102–107.

Liu, Q., Zhang, J.H., Zhang, H.R., Yao, F.M., Bai, Y., Zhang, S., Meng, X.L., Liu, Q., 2021. Evaluating the performance of eight drought indices for capturing soil moisture dynamics in various vegetation regions over China. Sci. Total Environ. 789 https://doi.org/10.1016/j.scitotenv.2021.147803.

Lorenz, C., Kunstmann, H., 2012. The hydrological cycle in three state-of-the-art reanalyses: Intercomparison and performance analysis. J. Hydrometeorol. 13, 1397–1420. https://doi.org/10.1175/JHM-D-11-088.1.

Lucht, W., Prentice, I.C., Myneni, R.B., Sitch, S., Friedlingstein, P., Cramer, W., Bousquet, P., Buermann, W., Smith, B., 2002. Climatic control of the high-latitude vegetation greening trend and Pinatubo effect. Science. 296, 1687–1689. https://doi.org/10.1126/science.

Ma, Z., 2007. The interdecadal trend and shift of dry/wet over the central part of North China and their relationship to the Pacific Decadal Oscillation (PDO). Chin. Sci. Bull. 52, 2130–2139. https://doi.org/10.1007/s11434-007-0284-z.

Ma, Z., Fu, C., 2003. Interannual characteristics of the surface hydrological variables over the arid and semi-arid areas of northern China. Glob. Planet. Chang. 37, 189–200. https://doi.org/10.1016/S0921-8181(02)00203-5.

Ma, B., Zhang, B., Jia, L.G., Huang, H., 2020. Conditional distribution selection for SPEI-daily and its revealed meteorological drought characteristics in China from 1961 to 2017. Atmos. Res. 246, 11. https://doi.org/10.1016/j.atmosres.2020.105108.

Ma, M.M., Zhang, X.J., Lyu, J., Su, Z.C.C.N.-11-5587/TV, 2021a. Research review and perspective of drought forecasting. China Flood Drought Manag. 31, 58–63. https://doi.org/10.16867/j.issn.1673-9264.2020412.

Ma, N., Szilagyi, J., Zhang, Y.Q., 2021b. Calibration-free complementary relationship estimates terrestrial evapotranspiration globally. Water Resour. Res. 57 https://doi.org/10.1029/2021WR029691. WE - Science Citation Index Expanded (SCI-EXPANDED).

Manzano, A., Clemente, M.A., Morata, A., Luna, M.Y., Begueria, S., Vicente-Serrano, S. M., Martin, M.L., 2019. Analysis of the atmospheric circulation pattern effects over SPEI drought index in Spain. Atmos. Res. 230, 1–11. https://doi.org/10.1016/j.atmosres.2019.104630.

Martens, B., Schumacher, D.L., Wouters, H., Munoz-Sabater, J., Verhoest, N.E.C., Miralles, D.G., 2020. Evaluating the land-surface energy partitioning in ERA5. Geosci. Model Dev. 13, 4159–4181. https://doi.org/10.5194/gmd-13-4159-2020.

McEvoy, D.J., Huntington, J.L., Mejia, J.F., Hobbins, M.T., 2016. Improved seasonal drought forecasts using reference evapotranspiration anomalies. Geophys. Res. Lett. 43, 377–385. https://doi.org/10.1002/2015gl067009.

McKee, T.B., Doesken, N.J., Kleist, J., 1993. The relationship of drought frequency and duration to time scales. In: Proceedings of the 8th Conference on Applied Climatology. American Meteorological Society Boston, MA, pp. 179–183.

Mishra, A.K., Singh, V.P., 2009. Analysis of drought severity-area-frequency curves using a general circulation model and scenario uncertainty. J. Geophys. Res. Atmos. 114, 1–18. https://doi.org/10.1029/2008JD010986.

Mishra, A.K., Singh, V.P., 2011. Drought modeling – A review. J. Hydrol. 403, 157–175. https://doi.org/10.1016/j.jhydrol.2011.03.049.

Mo, K.C., Lyon, B., 2015. Global meteorological drought prediction using the north american multi-model ensemble. J. Hydrometeorol. 16, 1409–1424. https://doi.org/10.1175/jhm-d-14-0192.1.

Mo, K.C., Schemm, J.K.E., Yoo, S.H., 2009. Influence of ENSO and the Atlantic Multidecadal Oscillation on Drought over the United States. J. Clim. 22, 5962–5982. https://doi.org/10.1175/2009jcli2966.1.

Morid, S., Smakhtin, V., Bagherzadeh, K., 2007. Drought forecasting using artificial neural networks and time series of drought indices. Int. J. Climatol. 27, 2103–2111. https://doi.org/10.1002/joc.1498.

Otkin, J.A., Anderson, M.C., Hain, C., Svoboda, M., 2015. Using temporal changes in drought indices to generate probabilistic drought intensification forecasts. J. Hydrometeorol. 16, 88–105. https://doi.org/10.1175/jhm-d-14-0064.1.

Park, S., Seo, E., Kang, D., Im, J., Lee, M.I., 2018. Prediction of drought on pentad scale using remote sensing data and MJO index through random forest over East Asia. Remote Sens. 10, 1–18. https://doi.org/10.3390/rs10111811.

Park, S., Im, J., Han, D., Rhee, J., 2020. Short-term forecasting of satellite-based drought indices using their temporal patterns and numerical model output. Remote Sens. 12, 1–21. https://doi.org/10.3390/rs12213499.

Quiring, S.M., 2009. Developing objective operational definitions for monitoring drought. J. Appl. Meteorol. Climatol. 48, 1217–1229. https://doi.org/10.1175/2009jamc2088.1.

Rippey, B.R., 2015. The U.S. drought of 2012. Weather Clim. Extrem. 10, 57–64. https://doi.org/10.1016/j.wace.2015.10.004.

Singer, M.B., Asfaw, D.T., Rosolem, R., Cuthbert, M.O., Miralles, D.G., MacLeod, D., Quichimbo, E.A., Michaelides, K., 2021. Hourly potential evapotranspiration at 0.1° resolution for the global land surface from 1981-present. Sci. Data 8, 224. https://doi.org/10.1038/s41597-021-01003-9.

Song, J.H., Kang, H.S., Byun, Y.H., Hong, S.Y., 2010. Effects of the Tibetan Plateau on the Asian summer monsoon: a numerical case study using a regional climate model. Int. J. Climatol. 30, 743–759. https://doi.org/10.1002/joc.1906.

Sun, G.H., Hu, Z.Y., Ma, Y.M., Xie, Z.P., Yang, S., Wang, J.M., 2020. Analysis of local land-atmosphere coupling in rainy season over a typical underlying surface in Tibetan Plateau based on field measurements and ERA5. Atmos. Res. 243, 1–12. https://doi.org/10.1016/j.atmosres.2020.105025.

Svoboda, M., LeComte, D., Hayes, M., Heim, R., Gleason, K., Angel, J., Rippey, B., Tinker, R., Palecki, M., Stooksbury, D., Miskus, D., Stephens, S., 2002. The drought monitor. Bull. Am. Meteorol. Soc. 83, 1181–1190. https://doi.org/10.1175/1520-0477(2002)083<1181:tdm>2.3.co;2.

Tateo, A., Miglietta, M.M., Fedele, F., Menegotto, M., Pollice, A., Bellotti, R., 2019. A statistical method based on the ensemble probability density function for the prediction of "Wind Days". Atmos. Res. 216, 106–116. https://doi.org/10.1016/j.atmosres.2018.10.001.

Tian, D., Martinez, C.J., 2012. Comparison of two analog-based downscaling methods for regional reference evapotranspiration forecasts. J. Hydrol. 475, 350–364. https://doi.org/10.1016/j.jhydrol.2012.10.009.

Trnka, M., Hlavinka, P., Mozny, M., Semeradova, D., Stepanek, P., Balek, J., Bartosova, L., Zahradnicek, P., Blahova, M., Skalak, P., Farda, A., Hayes, M., Svoboda, M., Wagner, W., Eitzinger, J., Fischer, M., Zalud, Z., 2020. Czech Drought Monitor System for monitoring and forecasting agricultural drought and drought impacts. Int. J. Climatol. 40, 5941–5958. https://doi.org/10.1002/joc.6557.

Vicente-Serrano, S.M., Begueria, S., Lopez-Moreno, J.I., 2010. A multiscalar drought index sensitive to global warming: The standardized precipitation evapotranspiration index. J. Clim. 23, 1696–1718. https://doi.org/10.1175/2009jcli2909.1.

Vicente-Serrano, S.M., Miralles, D.G., Dominguez-Castro, F., Azorin-Molina, C., El Kenawy, A., McVicar, T.R., Tomas-Burguera, M., Begueria, S., Maneta, M., Pena-Gallardo, M., 2018. Global assessment of the standardized evapotranspiration deficit index (SEDI) for drought analysis and monitoring. J. Clim. 31, 5371–5393. https://doi.org/10.1175/jcli-d-17-0775.1.

Wang, Z.Q., Duan, A.M., Wu, G.X., 2014. Time-lagged impact of spring sensible heat over the Tibetan Plateau on the summer rainfall anomaly in East China: case studies using the WRF model. Clim. Dyn. 42, 2885–2898. https://doi.org/10.1007/s00382-013-1800-2.

Wang, Y.X., Li, J.Z., Feng, P., Chen, F.L., 2015. Effects of large-scale climate patterns and human activities on hydrological drought: a case study in the Luanhe River basin. China. Nat. Hazards 76, 1687–1710. https://doi.org/10.1007/s11069-014-1564-y.

Wang, Q.F., Wu, J.J., Li, X.H., Zhou, H.K., Yang, J.H., Geng, G.P., An, X.L., Liu, L.Z., Tang, Z.H., 2017a. A comprehensively quantitative method of evaluating the impact of drought on crop yield using daily multi-scale SPEI and crop growth process model. Int. J. Biometeorol. 61, 685–699. https://doi.org/10.1007/s00484-016-1246-4.

Wang, S.S., Yuan, X., Li, Y.H., 2017b. Does a strong El Nino imply a higher predictability of extreme drought? Sci. Rep. 7, 1–7. https://doi.org/10.1038/srep40741.

Wang, Q., Zeng, J., Qi, J., Zhang, X., Zeng, Y., Shui, W., Xu, Z., Zhang, R., Wu, X., Cong, J., 2021. A multi-scale daily SPEI dataset for drought characterization at observation stations over mainland China from 1961 to 2018. Earth Syst. Sci. Data 13, 331–341. https://doi.org/10.5194/essd-13-331-2021.

Wells, N., Goddard, S., Hayes, M.J., 2004. A self-calibrating Palmer Drought Severity Index. J. Clim. 17, 2335–2351. https://doi.org/10.1175/1520-0442(2004)017<2335:ASPDSI>2.0.CO;2.

Whitaker, J.S., Hamill, T.M., Wei, X., Song, Y.C., Toth, Z., 2008. Ensemble data assimilation with the NCEP Global Forecast System. Mon. Weather Rev. 136, 463–482. https://doi.org/10.1175/2007mwr2018.1.

Wilhite, D.A., Svoboda, M.D., Hayes, M.J., 2007. Understanding the complex impacts of drought: A key to enhancing drought mitigation and preparedness. Water Resour. Manag. 21, 763–774. https://doi.org/10.1007/s11269-006-9076-5.

Wilks, D.S., 2006. Statistical methods in the atmospheric sciences, second ed. Academic Press, San Diego, Calif, p. 255.

Yang, L., Tian, F., Sun, Y., Yuan, X., Hu, H., 2014. Attribution of hydrologic forecast uncertainty within scalable forecast windows. Hydrol. Earth Syst. Sci. 18, 775–786. https://doi.org/10.5194/hess-18-775-2014.

Yuan, X., Wood, E.F., 2013. Multimodel seasonal forecasting of global drought onset. Geophys. Res. Lett. 40, 4900–4905. https://doi.org/10.1002/grl.50949.

Yuan, X., Wood, E.F., Roundy, J.K., Pan, M., 2013. CFSv2-based seasonal hydroclimatic forecasts over the conterminous United States. J. Clim. 26, 4828–4847. https://doi.org/10.1175/jcli-d-12-00683.1.

Zhang, Y.H., Li, W.W., Chen, Q.H., Pu, X., Xiang, L., 2017. Multi-models for SPI drought forecasting in the north of Haihe River Basin. China. Stoch. Environ. Res. Risk Assess. 31, 2471–2481. https://doi.org/10.1007/s00477-017-1437-5.

Zhang, X., Li, M.X., Ma, Z.G., Yang, Q., Lv, M.X., Clark, R., 2019. Assessment of an evapotranspiration deficit drought index in relation to impacts on ecosystems. Adv. Atmos. Sci. 36, 1273–1287. https://doi.org/10.1007/s00376-019-9061-6.

Zhang, X., Duan, Y.W., Duan, J.P., Jian, D.N., Ma, Z.G., 2021. A daily drought index based on evapotranspiration and its application in regional drought analyses. Sci. China Earth Sci. https://doi.org/10.1007/s11430-021-9822-y.

Zhang, Y., Mao, G., Chen, C., Shen, L., Xiao, B., 2021. Population Exposure to Compound Droughts and Heatwaves in the Observations and ERA5 Reanalysis Data in the Gan River Basin. China. L. 10 https://doi.org/10.3390/land10101021.

Zhao, Q.Y., Carr, F.H., 1997. A prognostic cloud scheme for operational NWP models. Mon. Weather Rev. 125, 1931–1953. https://doi.org/10.1175/1520-0493(1997)125<1931:apcsfo>2.0.co;2.

Zhu, Y.Q., Liu, E., Mahajan, R., Thomas, C., Groff, D., Van Delst, P., Collard, A., Kleist, D., Treadon, R., Derber, J.C., 2016. All-sky microwave radiance assimilation in NCEP's GSI analysis system. Mon. Weather Rev. 144, 4709–4735. https://doi.org/10.1175/mwr-d-15-0445.1.

Zou, X., Zhang, Q., Wang, Y., Gao, G., 2005. Drought indices and operational drought monitoring in the U. S.A. and China. Meteorol. Monogr. 31, 6–9.